Biobased Chemistry and Technology

BSc Thesis Biosystems Engineering

Modelling the Effects of Excretion Variations on Nutrient Dynamics in a Recirculating Aquaculture System

Jan-David Wacker

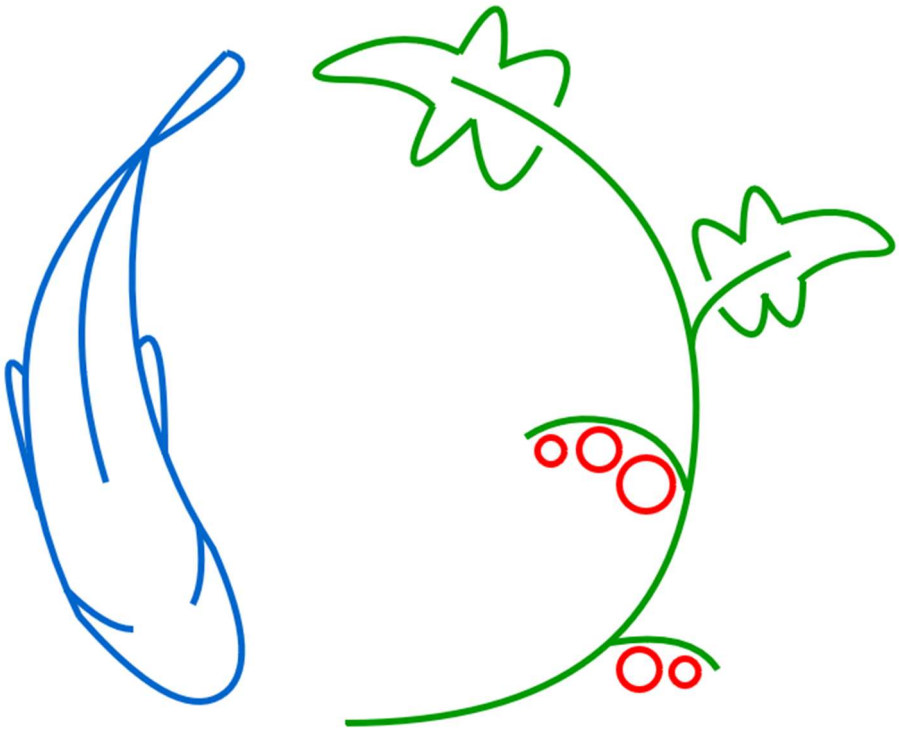

23-08-2018

WAGENINGEN
UNIVERSITY & RESEARCH

INAPRO

Name course	:	BSc Thesis Biosystems Engineering
Number	:	YEI-80324
Study load	:	24 ects
Date	:	23-08-2018

Student	:	Jan-David Wacker
Registration number	:	930525-923-080
Study programme	:	BAT
Report number	:	103BCT

Supervisor(s)	:	D Reyes Lastiri MSc, Prof.dr.ir KJ Keesman
Examiners	:	Prof.dr.ir KJ Keesman, ir. HJ Cappon
Group	:	Biobased Chemistry and Technology
Address	:	Bornse Weilanden 9 6708 WG Wageningen The Netherlands

WAGENINGEN
UNIVERSITY & RESEARCH

Abstract

Aqauponics is the combination of fish and plant cultivation. To improve balancing between optimal growth requirements of fish and plants, dynamics of nutrients relevant for plant growth need to be known. This study investigated on the dynamics of ammonia, nitrate, phosphorus, potassium, calcium, magnesium and sodium in the aquaculture loop of an auquaponic system, cultivating tilapia and tomatoes. Special interest was given to the diurnal excretion variations of the fish. For general applicability of the model a wide set of data was used to calibrate model parameters. It was found that the excretion variations affect the performance of all system modules. Particulate nutrient concentrations in the fish tank peak one hour after feeding, soluble nutrient concentration 2.5 hours later. A daily maximum is reached after the last feeding of the day. Model outputs were compared to data from a comparable system. The deterministic model was not able to accurately represent the system. Implementation of the estimated parameter uncertainties is required.

Contents

1. Introduction

Aquaculture is considered one of the worlds fastest growing food production sectors (FAO, 2016). In recirculating aquaculture systems (RAS) fish can be raised in high densities with minimal external influences. However, recirculation of water leads to accumulation of fish excreta, which can build up to stressful or toxic levels. Different filtration techniques are applied in RAS to remove the excreta from the recirculating water (Timmons and Ebeling, 2013).

In fish physiology, ammonia is the main excretion form of protein metabolites. Due to the toxicity of ammonia, biological filters with nitrifying bacteria are used in RAS, to turn ammonia into less harmful nitrate (Eding et al., 2006). Nitrate-N is a macro-nutrient in plant nutrition. In the 1970's aquaculture researchers proposed therefore the use of plants for removing nitrate from RAS water (Lewis et al., 1978).

Soilless plant cultivation, where plants receive all required nutrients via irrigation, is called hydroponics. Aquaponics is a symbiotic combination of aquaculture and hydroponics, where plants take up nutrients excreted by fish. In an aquaponic system fish can benefit from improved water quality, and plant cultivation will require less external fertilisers (J. E. Rakocy, 2012). However, as of now aquaponic systems are not yet present on a commercial scale (Love et al., 2015).

A major challenge in aquaponics lies in the balancing between optimal growth conditions of fish, nitrifying bacteria and plants (Goddek, 2017). To tackle this problem Kloas et al. (2015) introduced decoupled aquaponics. Instead of letting the water recirculate through RAS and hydroponics, in decoupled aquaponics RAS and hydroponics form two separate recirculating loops. Only part of the nutrient rich water from the RAS loop is sent to the hydroponic loop. By separating fish and plant cultivation in an aquaponic system, the trade-offs that have to be made between the two can be minimised.

With the aim to raise aquaponics on a commercially competitive level, the European Union provides funding towards a research project entitled INAPRO (Innovative Aquaponics for Professional Applications) (Kloas et al., 2015). Goal of the INAPRO project is a model-based optimisation of decoupled aquaponic systems. Factors pending for improvement are water reuse and nutrient recovery, together with a minimisation of waste effluents and energy demand. The project focusses on the cultivation of Nile tilapia (*Oreochromis niloticus*) in RAS combined with the cultivation of tomatoes (*Solanum lycopersicum*) in a hydroponic system (INAPRO, n.d.).

1.1. System description

The decoupled aquaponic system under investigation in the INAPRO project has a modular setup (1.1).

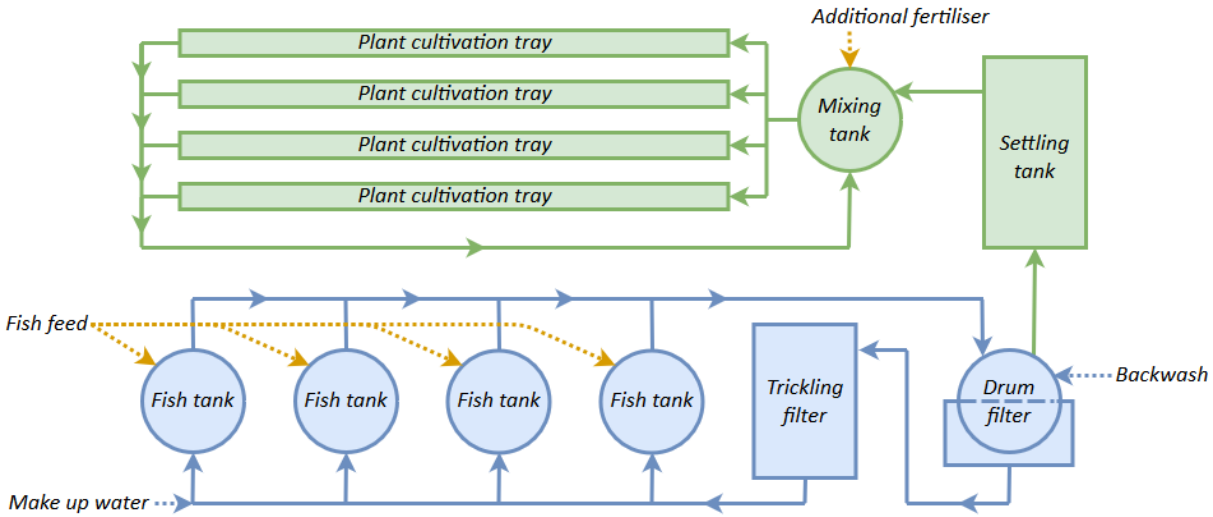

Figure 1.1.: Schematic illustration of a decoupled aquaponic system consisting of a RAS loop (solid blue lines) and a hydroponic loop (solid green lines), with water inflows (dotted blue lines) and nutrient inputs (dotted yellow lines)

In the aquaculture loop, fish are cultivated in rearing tanks. To maintain an appropriate water quality, flow rates of the recirculating water stream should result in hydraulic retention times of approximately one hour in each fish tank (Losordo et al., 2000). The waste water is filtered mechanically and biologically before it returns to the fish tanks. For mechanical filtration microscreen drum filters are commonly used to remove particulate solids larger than 40 to 100 µm (Tucker and Hargreaves, 2008). To turn the toxic ammonia into less harmful nitrate, a trickling filter with nitrifying bacteria is used.

Solids removed by the drum filter are backwashed towards the hydroponic loop. Due to the relatively small flow rate, a settling tank is appropriate to remove solids by sedimentation (Timmons and Ebeling, 2013). Afterwards the water is collected in a mixing tank, wherein the nutrients, lacking for optimal plant growth, are added. The nutrient rich water recirculates through cultivation trays from which the plants take up water and nutrients.

1.2. Problem description

Aquaponics is a promising food production technique. However, an aquaponic system that can economically compete with separate aquaculture and horticulture systems, has yet to be found. The main challenge lies in finding a balance between the requirements of fish and plants. Nutrient concentrations in the aquaculture water must not exceed levels stressful or toxic to fish, and at the same time nutrient concentrations in the hydroponic water must meet the requirements for optimal plant growth.

Both fields, RAS and hydroponics, are vastly researched. However when combining the two, new interests arise. In RAS water treatment the focus lies on the removal of ammonia and particulate solids. The accumulation of these two form the biggest threats to fish well-being (Timmons and Ebeling, 2013). Physical properties, composition, and dynamics of RAS waste streams are of minor interest for aquaculture researchers.

In a decoupled aquaponic system these waste streams become inputs to the hydroponic loop. Tomatoes growing in a hydroponic system require water flows with a range of soluble nutrients, mainly Nitrogen (N), Phosphorus (P), Potassium (K), Calcium (Ca), and Magnesium (Mg). An excess of Sodium (Na) on the other hand, can inhibit plant growth (Ross, 1998). It is therefore important to track down the dynamics of these nutrients in the RAS loop, in both forms, soluble and particulate.

The main nutrient input of the RAS loop is fish feed. It is recommended to feed tilapia three to six times per day, depending on the age (Wing-Keong and Romano, 2013). These feeding frequencies lead to diurnal variations in fish excretions. Taking the diurnal excretion variations into account is crucial when investigating nutrient dynamics in RAS. Oscillating nutrient concentrations can temporarily exceed levels comfortable for fish (Eding et al., 2006).

For deeper understanding and optimisation of complex systems mathematical models are commonly applied. Several models of decoupled aquaponics have been developed. However, all of them have limitations. Goddek (2017), Karimanziraa et al. (2016), and Reyes Lastiri et al. (2016) for example focus only on two or three of the relevant nutrients. The only model including all six previously named nutrients, is the one developed by Reyes Lastiri et al. (2018). This model, however, doesn't account for diurnal excretion variations.

In conclusion, the problem this study focuses on is the scarcity of knowledge regarding the dynamics of nutrients relevant for plant growth in RAS, even though there has been extensive research done on RAS and aquaponics. To achieve a commercial breakthrough, an aquaponic system must meet optimal growth requirements of fish and plants. Therefore, the dynamics of soluble and particulate nutrients in the RAS loop must be known. When looking at the nutrient dynamics, it is important to account for diurnal excretion variations of fish. A model describing these dynamics and accounting for diurnal excretion variations of the fish doesn't exist yet.

1.3. Objectives

To tackle the stated problem, this study aims to determine dynamics of soluble and particulate nutrients in the RAS loop of decoupled aquaponic systems, and to identify the effect of diurnal excretion variations on these. For further improvement of aquaponics and related models, uncertainties and bottlenecks corresponding to the nutrient dynamics need to be located. The focus lies on N, P, K Ca, Mg and Na. As part of the INAPRO project, the objective of this study is the development of a widely applicable model, with separate submodels for the following system modules: feeder, fish, fish tank, drum filter, trickling filter and settling tank.

Research questions of the current study are:

1. What are the effects of excretion variations on nutrient concentrations and module performance in the RAS loop of a decoupled aquaponic system?
2. What are the main uncertainties and bottlenecks in modelling the nutrient dynamics for each module and how can submodels be improved?

1.4. Approach

The program chosen for modelling is Python™. For each of the following system modules submodels are constructed: feeder, fish, fish tank, drum filter, trickling filter and settling tank. Based on mass balances, each submodel describes the dynamics of soluble and particulate nutrients in the corresponding system module. Submodels must be complex enough to predict diurnal variations in nutrient concentrations, yet they must be general enough to allow application on a full system level.

Submodel parameters are estimated, so that they represent the physiology of Nile tilapia, as well as the physical properties and filtration performance of system modules. This is done by calibrating the submodels against data taken from literature. Parameter estimation and system simulations are used to identify uncertainties and bottlenecks.

1.5. Outline

In chapter 2 the constructed model is explained per system module. Model parameters are estimated in chapter 3. The results of different simulations are shown and discussed in chapter 4, an uncertainty analysis for the fish module is also presented. In chapter 5 a general discussion and conclusions per system module are shown.

2. Model Identification

To describe the dynamics of soluble and particulate nutrients in the RAS loop of a decoupled aquaponic system (figure 1.1), a dynamic, modular model was constructed. For each system module submodels were defined. In this chapter system modules and their submodels are described in the order shown in table 2.1.

Table 2.1.: Modules of the RAS loop of a decoupled aquaponic system and corresponding submodels described in this chapter

Section	Module	Submodel
2.1	Feeder	Feeding levels depending on fish weight
2.2	Fish	Digestion and excretion dynamics
2.3	Fish tank	Dynamics of excreted nutrients
2.4	Drum filter	Filtration efficiency and effect on particle size distribution
2.5	Trickling filter	Nitrification dynamics
2.6	Settling tank	Solids removal efficiency

Nutrients observed in this study are nitrate nitrogen ($NO_3^- - N$), total ammonia nitrogen ($TAN - N$), phosphate phosphorus (PO_4^{3-}), potassium (K^+), calcium (Ca^{2+}), magnesium (Mg^{2+}), and sodium (Na^+). The following abreviations are used for these nutrients: NO_3, TAN, P, K, Ca, Mg, and Na. Another component of interest is the concentration of total suspended solids (TSS). To differentiate between soluble and particulate phases of nutrients, a notation following the standard in wastewater treatment is used, where X stands for all concentrations of particulate matter and S for all concentrations of soluble substances (Grau et al., 1983).

All submodels are based on mass balances, with the assumption that all water flows have a density of 1000 kg/m^3, regardless of their soluble substance and particulate matter concentration. The only chemical process considered is nitrification, which is assumed to only take place in the trickling filter. Differential equations are solved with the Euler Forward method. Integrals are calculated with the python function scipy.integrate.cumtrapz, which uses the trapezodial rule. The time step used for all submodels is 15 min.

Submodels were constructed to represent the physiology of Nile tilapia and/or physical properties of the corresponding system module. To give a somewhat transparent model rather than a black box model, it was tried to construct submodels in such a way, that all relevant parameters have a physical meaning. On the other hand, complex submodels were avoided, to guarantee a system level approach. The transparency and modularity of the model also allows easy adaptation to different system set-ups

The programming language chosen for modelling is Python™, due to its simplicity and fortitude. The overall model follows an object oriented programming paradigm, where each

submodel is an object, independent of other model parts. This supports the modularity of the model. Furthermore is Python™ an open source software and therefore readily accessible. Accessibility and adaptability give a universal model that can be easily applied to various aquaponic systems and facilitate future use of the model.

2.1. Feeder

Fish feed is the main nutrient and solids input to the RAS loop. To maximise fish growth and minimise faecal excretions, the feed formulation has to meet the nutritional requirements of the cultured fish (Tucker and Hargreaves, 2008). In table 2.2 the nutritional content of Tilapia feed is shown.

Table 2.2.: Tilapia diet formulation in g/kg feed (wet weight)

Component	Composition
Dry matter	885.59 (±19.48)
Crude protein	325.92 (±51.90)
C	400.97 (±7.36)
N	51.20 (±7.91)
P	12.44 (±2.14)
K	13.96 (±1.40*)
Ca	23.52 (±4.28)
Mg	3.27 (±0.33*)
Na	5.13 (±0.51*)

Values are means of data reported by Schneider et al. (2004), Neto and Ostrensky (2015), and Seawright et al. (1998);
N = protein/6.25;
Uncertainties are standard errors of means;
* Uncertainty assumed to be 10% of nominal value;
See table A.1 for full dataset

To save labour costs automatic feeders are commonly used in intensive aquaculture. They allow precise regulation of feeding levels and frequencies (DeLong et al., 2009). Feeding levels are an important factor; if they are too low, fish growth will be reduced and aggression between fish might be induced. On the other hand, feeding in excess leads to a lower feed utilisation, which in turn, lowers the economic performance. It is therefore recommended to feed a daily percentage of the body weight dependent on the growth stage. Recommended feeding frequencies are three to six times per day, for optimal feed utilisation (Wing-Keong and Romano, 2013). A spread out feeding schedule also results in less oscillation of water quality parameters (Tucker and Hargreaves, 2008).

Young fish (fry) require the highest feeding ratios relatively to their body mass, due to high growth rates. This decreases to a stable feeding rate of 1.5 to 3% of body mass per day, as is recommended for fish larger than 75 g (DeLong et al., 2009). The optimal daily

feeding ratio (DFR) depending on fish weight throughout all growth stages can best be described by a power-law function:

$$DFR = a_{DFR} * m_{fish,ideal}{}^{b_{DFR}} \tag{2.1}$$

Where the DFR is a percentage of body mass that should be fed per day, it depends on the body mass (wet weight) $m_{fish,ideal}$ and the two constants a_{DFR} and b_{DFR}.

Since the DFR depends on the fish weight, an automatic feeder also needs a simple ideal fish growth model, to estimate the required amount of feed. It has been shown that quadratic models are appropriate to predict the growth of tilapia (Amanico et al., 2014), see equation 2.2.

$$m_{fish,ideal} = a_{growth} * t + b_{growth} * t^2 \tag{2.2}$$

Function 2.2 predicts fish body mass m dependent on time t and the two constants a_{growth} and b_{growth}.

Knowing the daily feeding ratio and the ideal fish weight, the feeder sub-model can estimate the required amount of feed per feeding (equation 2.3):

$$f_{m,feed}(t) = \begin{cases} \frac{DFR * m_{fish,ideal}}{n_{feedings}} * \frac{1}{dt_{feeder}} & \text{if } t = t_{feeding} \\ 0 & \text{otherwise} \end{cases} \tag{2.3}$$

Where $f_{m,feed}$ stands for the mass flow of feed, $n_{feedings}$ for the number of feedings per day, dt_{feeder} for the simulation time of the feeder and $t_{feeding}$ for all times at which feedings are scheduled. Feed is only distributed at scheduled feeding times. The feed mass flow is therefore modelled as an impulse.

With the proposed submodel for the feeder module, feeding levels can be estimated. By relying on its own simple fish growth model, this submodel can operate independent of the fish submodel.

2.2. Fish

With an ideal feeding regime it is assumed that all feed provided is consumed by the fish. Consumed feed travels through the fish's intestines. For simplification and modelling purposes, the fish's intestines are seen as two separate storing tanks, namely the digestive tract (stomach and guts) and the urinary tract (kidneys and liver). Nutrients consumed by the fish via feed, leave the digestive and urinary tracts eventually in three forms: body tissue deposition (uptake), faeces (particulate excreta), and urine (soluble excreta).

Digestible feed contents are metabolised in the digestive tract, and partly taken up as body tissues. Indigestible feed contents travel unaffected through the digestive tract and leave it as particulate excreta in the form of faeces. Not-retained metabolism products are excreted as soluble excreta (Neto and Ostrensky, 2015). It is assumed that all soluble excreta are in the form of urine, which is excreted from the urinary tract. In figure 2.1 an illustration of the described nutrient flows is shown.

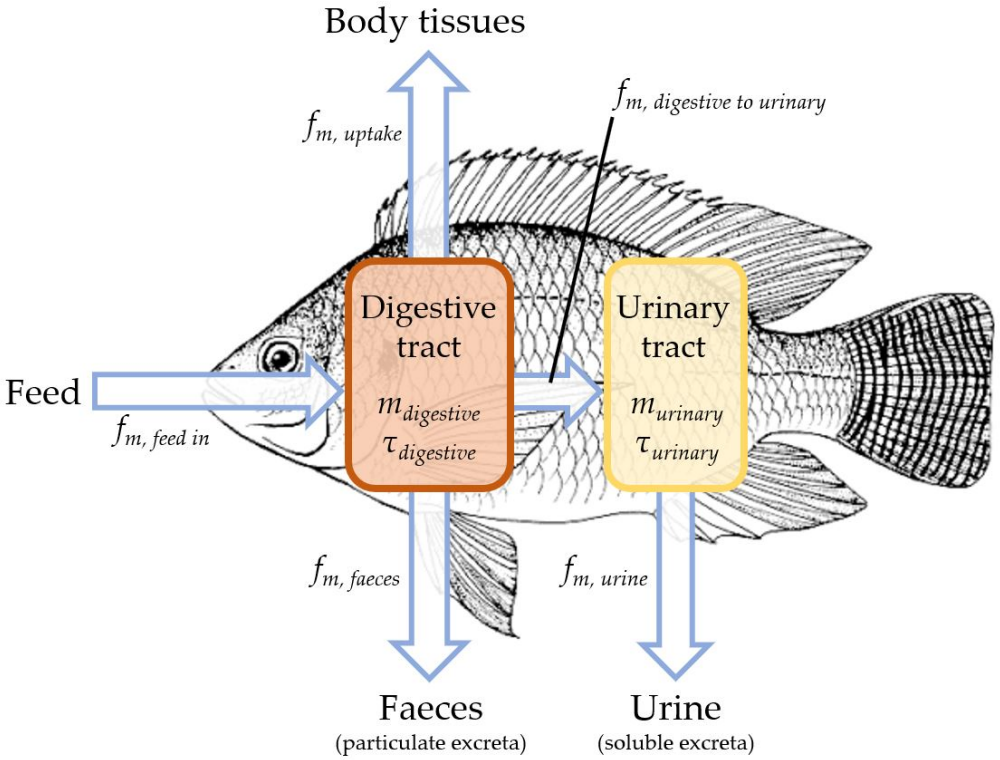

Figure 2.1.: Schematic illustration of mass flows within a fish; Digestive tract and urinal tract are seen as two storage tanks; Tilapia figure from FAO (2005).

To describe the nutrient flows in the fish's digestive tract, a first order differential equation (equation 2.4) is used.

$$\frac{\mathrm{d}m_{digestive}}{\mathrm{d}t} = f_{m,feed} - f_{m,digestive,out} \tag{2.4}$$

Where $\frac{dm_{digestive}}{dt}$ is the change in mass of the digestive tract contents. It is the difference between the mass flow entering the digestive tract via feed ($f_{m,feed}$) and the mass flow leaving the digestive tract ($f_{m,digestive,out}$). The latter can be calculated by multiplying the mass of digestive tract contents by its inverted time-constant ($\tau_{digestive}$), see equation 2.5. The time constant determines the rate of evacuation.

$$f_{m,digestive,out} = \frac{1}{\tau_{digestive}} * m_{digestive} \tag{2.5}$$

The flow out of the digestive tract splits up into a uptake flow, a faeces flow and a flow to the urinary tract. The balance of these flows is displayed in equation 2.6. The three resulting mass flows can also be described as fraction of the mass flow out of the stomach, see equation 2.7. The fractions k_{uptake}, k_{faeces} and k_{urine} add up to one.

$$f_{m,digestive,out} = f_{m,faeces} + f_{m,uptake} + f_{m,digestive \rightarrow urinary} \tag{2.6}$$

$$\begin{aligned} f_{m,uptake} &= k_{uptake} * f_{m,digestive,out} \\ f_{m,faeces} &= k_{faeces} * f_{m,digestive,out} \\ f_{m,digestive \rightarrow urinary} &= k_{urine} * f_{m,digestive,out} \end{aligned} \tag{2.7}$$

For the nutrient flows in the fish's urinary tract, a first order differential equation (equation 2.8) is likewise used, where the change in its contents mass is equal to the mass coming in from the digestive tract ($f_{m,digestive \rightarrow urinary}$), minus the mass flowing out ($f_{m,\ urine}$). All nutrients in the urinary tract are eventually excreted as urine, the emptying rate depends on the time constant ($\tau_{urinary}$), see equation 2.9.

$$\frac{\mathrm{d}m_{urinary}}{\mathrm{d}t} = f_{m,digestive \rightarrow urinary} - \frac{1}{\tau_{urinary}} * m_{urinary} \tag{2.8}$$

$$f_{m,\ urine} = \frac{1}{\tau_{urinary}} * m_{urinary} \tag{2.9}$$

From each consumed nutrient, different percentages are retained or excreted by the fish. Balances between the nutrient mass flows leaving the digestive and urinal tract are shown in table 2.3.

Table 2.3.: Intra-corporeal nutrient balance for tilapia as percentage of nutrient consumed

Nutrient	Uptake ratio	Faeces ratio	Urine ratio
C	33.28 (±1.82)	15.43 (±1.11)	51.28 (±1.13)
N	44.40 (±1.85)	11.16 (±3.10)	44.44 (±2.92)
P	53.18 (±13.08)	43.32 (±8.22)	3.49 (±13.71)
K	24.25 (±1.09)	4.25 (±1.30)	71.50 (±0.87)
Ca	36.96 (±3.70*)	26.10 (±4.88)	36.94 (±4.88)
Mg	20.50 (±1.12)	18.50 (±3.64)	61.00 (±2.83)
Na	50.00 (±5.15)	13.00 (±3.54)	37.00 (±8.34)

Values are means of data reported by Schneider et al. (2004), Neto and Ostrensky (2015) and Seawright et al. (1998);
Urine ratios are calculated as difference closing the nutrient balance;
Uncertainties are standard errors of means;
* Uncertainty assumed to be 10% of nominal value;
See table A.4 to A.6 for full dataset

The mass flows of each nutrient leaving the fishes intestines are calculated as shown in equation 2.10, *Nutr.* stands representative for all seven nutrients listed in table 2.3.

$$f_{m,Nutr.,uptake} = x_{Nutr.,feed} * k_{Nutr.,uptake} * f_{m,digestive,out} \tag{2.10}$$

$$f_{m,Nutr.,faeces} = x_{Nutr.,feed} * k_{Nutr.,faeces} * f_{m,digestive,out} \tag{2.11}$$

$$f_{m,Nutr.,urine} = x_{Nutr.,feed} * k_{Nutr.,digestive \rightarrow urinal} * f_{m,digestive,out} \tag{2.12}$$

Where $f_{m,Nutr.,uptake}$ stands for the mass flow of each nutrient that is retained as body mass, $f_{m,Nutr.,faeces}$ for the mass flow of each nutrient that is excreted as faeces and $f_{m,Nutr.,urine}$

for the mass flow of each nutrient that is excreted as urine. The percentage of each nutrient in the feed is expressed by $x_{Nutr.,feed}$. Which fraction of the consumed nutrient is taken up, excreted as faeces or excreted as urine, is determined by the ratios listed in table 2.3 and expressed by $k_{Nutr.,uptake}$, $k_{Nutr.,faeces}$ and $k_{Nutr.,urine}$.

With the model proposed for the fish module, dynamics of uptake and excretion can be estimated in total as well as per nutrient. By splitting the excretion up into a urine and a faeces flow, differentiation between soluble and particulate excreta can be made. Feed enters the fish as an impulse input, by modelling the digestive and urinal tract as storage tank excretion is stretched over a much longer time span.

2.3. Fish Tank (FT)

The fish are cultivated in a fish tank, which is seen as a continuously stirred tank with a constant volume (V_{FT}). Soluble ($f_{m,urine}$) and particulate excreta ($f_{m,faeces}$) of the fish accumulate in the water. A constant flow leaves the fish tank towards the drum filter ($f_{V,FT,out}$), an equally sized flow enters the fish tank. When the flow coming in from the trickling filter ($f_{V,TF,out}$) is smaller than the outflow, a fresh water inflow ($f_{V,FT,fresh}$) is added (equation 2.13). In figure 2.2 an illustration of the fish tank model is shown. X and S denote the concentrations of particulate matter and soluble substances in the corresponding system module.

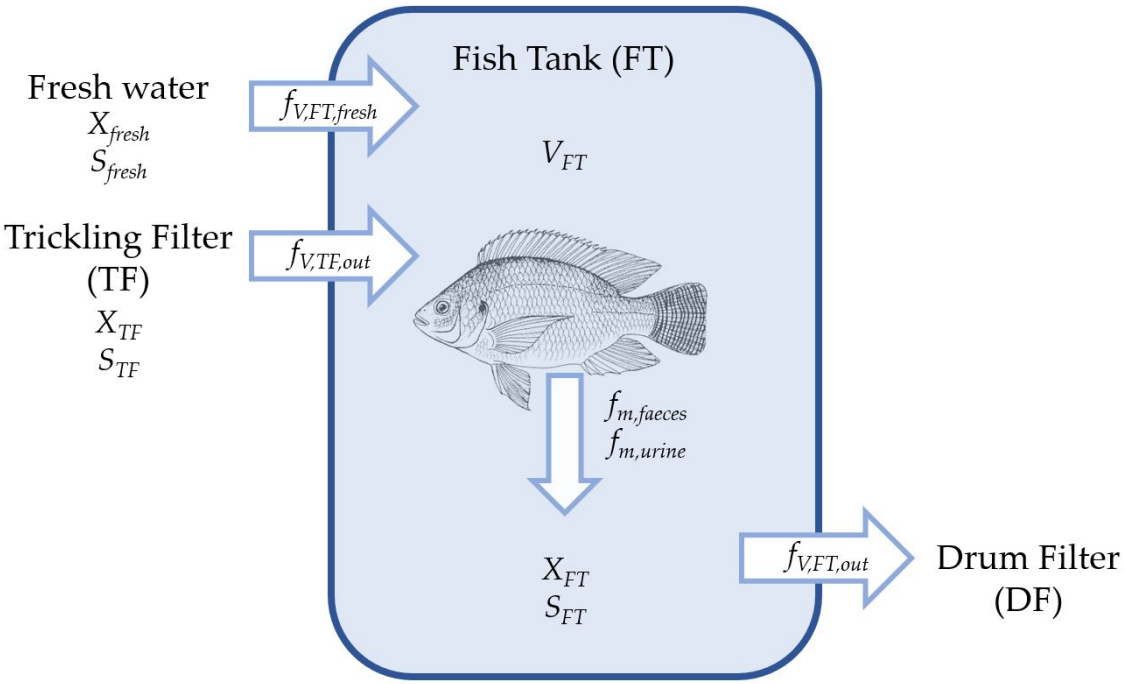

Figure 2.2.: Schematic illustration of fish tank model; X stands for all particulate matter concentrations; S stands for all soluble matter concentrations; Tilapia figure from FAO (2005).

$$f_{V,FT,out} = f_{V,TF,out} + f_{V,FT,fresh} \tag{2.13}$$

To describe the mass change of particulate matter concentrations ($\frac{\mathrm{d}X_{FT}}{\mathrm{d}t}$) and soluble matter concentrations ($\frac{\mathrm{d}S_{FT}}{\mathrm{d}t}$) in the fish tank, two first order differential equations are used (equation 2.14 and 2.15).

$$\frac{\mathrm{d}X_{FT}}{\mathrm{d}t} = \frac{1}{V_{FT}} * (X_{TF} * f_{V,TF,out} + X_{fresh} * f_{V,FT,fresh} + f_{m,faeces} - X_{FT} * f_{V,FT,out}) \tag{2.14}$$

$$\frac{\mathrm{d}S_{FT}}{\mathrm{d}t} = \frac{1}{V_{FT}} * (S_{TF} * f_{V,TF,out} + S_{fresh} * f_{V,FT,fresh} + f_{m,urine} - S_{FT} * f_{V,FT,out}) \tag{2.15}$$

By modelling the fish tank as a continuously stirred tank, soluble and particulate excreta of the fish are diluted by the fish tank water, before they are eventually carried out towards the drum filter. Since RAS fish tanks typically have a hydraulic retention time of one hour (Losordo et al., 2000), soluble substances and particulate matter leaving the fish tank are modelled with a delay time of one hour.

2.4. Drum Filter (DF)

To maintain a water quality, appropriate for the cultivation of fish, it is important to constantly remove suspended solids from the RAS water stream. For tilapia, the concentration of total supended solids (TSS) should not exceed 30 mg/L (Timmons and Ebeling, 2013). Micro-screen filtration is the most popular solids removal technology used in RAS (Tucker and Hargreaves, 2008). Screen apertures of $60 - 100$ μm were found to be most efficient (Kelly et al., 1997).

Drum filters are a commonly used application of micro-screen filtration, in which the bulk water-flow is forced to travel through a cylinder shaped sieve. The water flow fills the cylinder only partially. By revolving around its own axis the sieve cylinder lifts captured solids (cake) above the water level, from where they are removed with a high pressure backwash flow. Backwash and cake form the retentate, which leaves the RAS loop. The operation of a micro-screen drum filter is illustrated in figure 2.3.

The operation of a drum filter can be seen as two steps. First, a fraction of the water flow coming in from the fish tank ($f_{V,DF,in}$) is captured by the micro-sieve. The captured fraction is called cake. The not captured fraction leaves the drum filter towards the trickling filter (equation 2.16). Then, a backwash water flow ($f_{V,backwash}$) is added to the cake flow ($f_{V,cake}$). Together they form the retentate ($f_{V,retentate}$), which flows to the settling tank (equation 2.17). A usual backwash flow is 1 % of the drum filter inflow (Summerfelt et al, 2001 cited in Tucker and Hargreaves 2008). Compared to the flow through the drum filter, its volume is insignificantly small, the model is therefore based on simple mass-balances. A schematic illustration of the model can be seen in figure 2.4.

$$f_{V,DF,out} = f_{V,DF,in} - f_{V,cake} \tag{2.16}$$

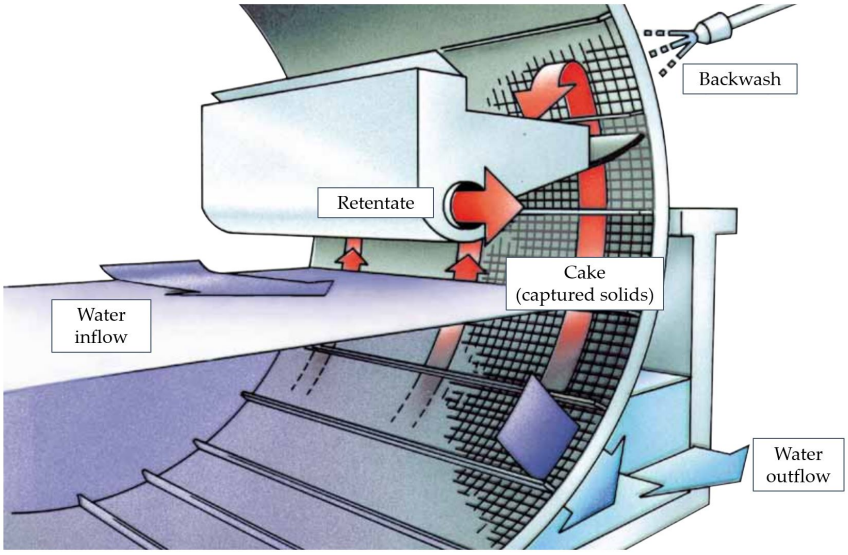

Figure 2.3.: Micro-screen drum filter operation; figure adapted from Hydrotech AB (n.d.). "HDF Drumfilters. Pure filtration in tough environments.". Vellinge, Sweden.

$$f_{V,retentate} = f_{V,cake} + f_{V,retentate} = 0.01 * f_{V,DF,in} + f_{V,retentate} \tag{2.17}$$

To calculate the volumetric flow of the cake, one needs to know the total suspended solids content in the cake (TSS_{cake}), see equation 2.18). The value for TSS_{cake} is estimated in section 3.3.2.

$$f_{V,cake} = \frac{f_{m,TSS,cake}}{TSS_{cake}} \tag{2.18}$$

Where $f_{m,TSS,cake}$ is the total mass flow of particulate solids, captured by the drum filter, which depends on the solids removal efficiency of the drum filter (η_{DF}) and the concentration of total suspended solids in the inflow (TSS_{FT}), see equation 2.19. The solids removal efficiency is identified in section 3.3.1. TSS_{FT} is the sum of all particulate solids concentrations in the fish tank.

$$f_{m,TSS,cake} = \eta_{DF} * TSS_{FT} * f_{V,DF,in} \tag{2.19}$$

The concentration of particulate matter in the flow leaving the drum filter towards the trickling filter ($X_{DF,out}$), in the cake (X_{cake}), and in the retentate ($X_{retentate}$) is calculated as shown in equations 2.20 to 2.22.

$$X_{DF,out} = \frac{1}{f_{V,DF,out}} * (1 - \eta_{DF}) * X_{FT} * f_{V,DF,in} \tag{2.20}$$

$$X_{cake} = \frac{1}{f_{V,cake}} * \eta_{DF} * X_{FT} * f_{V,DF,in} \tag{2.21}$$

$$X_{retentate} = \frac{1}{f_{V,retentate}} * (X_{cake} * f_{V,cake} + X_{backwash} * f_{V,backwash}) \tag{2.22}$$

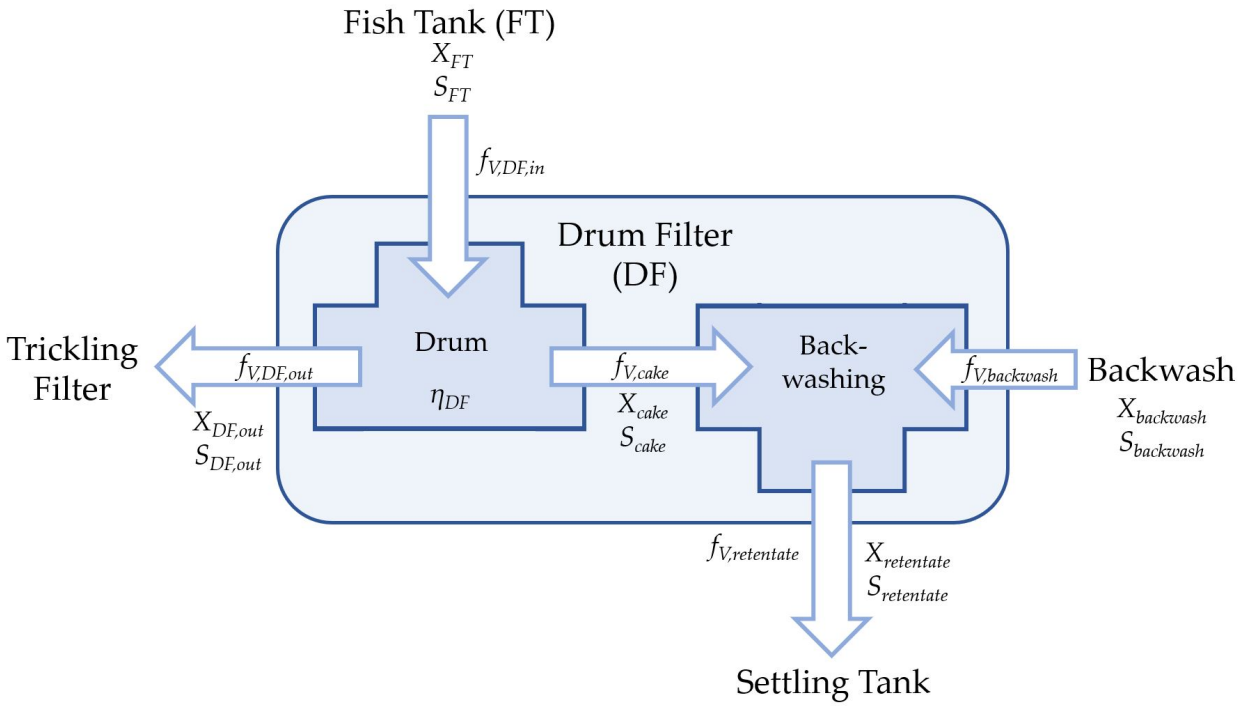

Figure 2.4.: Schematic illustration of the drum filter model; X stands for all particulate solids concentrations; S stands for all soluble matter concentrations

The concentrations of soluble matter in the drum filter outflow ($S_{DF,out}$) and the cake (S_{cake}) are the same as in the drum filter inflow (S_{FT}). In the retentate ($S_{retentade}$), soluble matter coming in with the backwash ($S_{backwash}$) is added to the soluble matter from the cake (equation 2.23).

$$S_{retentate} = \frac{1}{f_{V,retentate}} * (S_{cake} * f_{V,cake} + S_{backwash} * f_{V,backwash}) \tag{2.23}$$

2.4.1. Particle Size Distribution

The majority of suspended solids in RAS are fine solids, with a particle size less than 100 µ m. Chen et al. (1993) found that particles smaller than 30 µ m in diameter represented 70-80% of the total weight of solids in a RAS fish tank. To describe the particle size distribution (PSD) in natural collections of small particles, Bader (1970) proposed the use of a power law function. This function has been adapted, to account for several particle size ranges (equation 2.24), where N_i stands for the number of particles, and $\bar{d}_i$ for the median particle diameter in size range i. A and β are two constants.

$$N_i = A\bar{d}_i^{-\beta} \tag{2.24}$$

When taking the logarithm on both sides of equation 2.24, β becomes the negative slope of the function (equation 2.25). The slope gives an appropriate characterization of the particle size distribution. The higher the negativity of the slope is, the more small particles

are present. Patterson et al. (1999) applied a comparable power law function to 10 different RAS, and found β-values ranging from 3.0 to 6.3.

$$\log N_i = \log A - \beta \log \bar{d}_i \tag{2.25}$$

Micro-screen filters remove particles larger than the screen apertures (Tucker and Hargreaves, 2008). After micro-screen filtration, the ratio of small particles in the water stream will be higher than before. It is therefore proposed to describe the drum filter performance with an increase of the β-value (equation 2.26). $\Delta\beta_{DF}$ is estimated in section 3.3.3.

$$\Delta\beta_{DF} = \beta_{afterDF} - \beta_{beforeDF} \tag{2.26}$$

With the model constructed for the drum filter all volumetric flows leaving the drum filter can be calculated, as well as the concentrations of soluble substances and particulate matter in these flows. In the drum filter the water stream recirculating through the RAS loop is reduced by the filtration. To make up for this water loss, a fresh water flow equal to the cake flow needs to be added to the fish tank. Further it is proposed to describe the drum filter performance by its effect on the particle size distribution.

2.5. Trickling Filter (TF)

90% of all soluble N excreta of fish is ammonia (Timmons and Ebeling, 2013). This makes it the main excretion form of fish protein metabolism. Ammonia is highly toxic to fish, the total ammonia-N (TAN) concentration in the fish-tank should not exceed 3 mg/l at any given time (Timmons and Ebeling, 2013). To decompose ammonia excretions of the fish, biofilters with nitrifying bacteria are used in RAS. Nitrifying bacteria turn ammonia into less harmful nitrate, for tilapia the upper limit of nitrate-N concentration is 400 mg/l (DeLong et al., 2009). When ignoring the formation of biomass, nitrification can be described by formula 2.27. Which shows that ammonia-N reacts to nitrate-N, on a one-to-one proportion.

$$NH_4^+ + 2O_2 + 2HCO_3^- \longrightarrow NO_3^- + 3H_2O + 2CO_2 \tag{2.27}$$

Trickling filters are an application of bio-filtration, commonly used in RAS. They are vertical towers, filled with an airy medium. Eding et al. (2006) advise filter heights of 2-4 m, they also report void space and specific surface area of different media to be around 90% and 200 m^2/m^3. The nitrifying bacteria grow on the medium surface. Water flows downwards through the medium. For the supply of oxygen, the filter needs to be aerated constantly.

Nijhof (1995) proposed a plug-flow model to describe the nitrification dynamics of a trickling filter applied in RAS. This model has been simplified to a series of 5 evenly spaced contentiously stirred tank reactors (CSTR). A schematic illustration of the trickling filter model can be seen in figure 2.5.

A continuous flow through the trickling filter is assumed, which means that the volumetric flow at any position of trickling filter is equal to the inflow ($f_{V,TF,in}$), see equation 2.28.

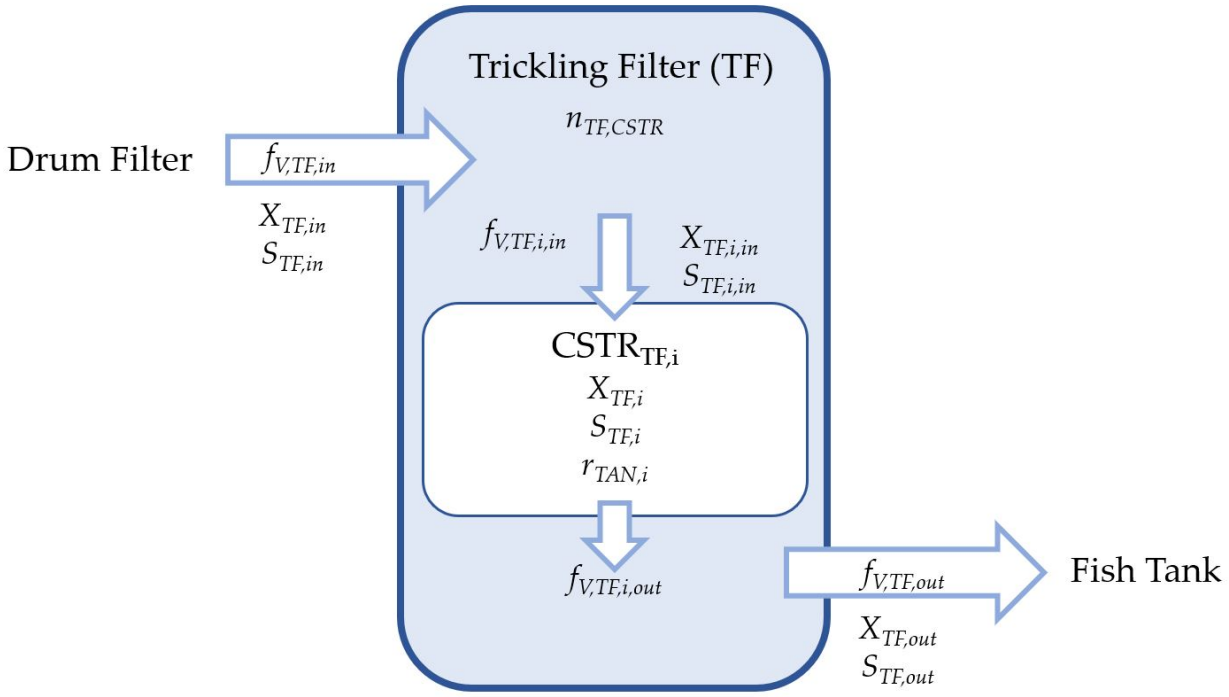

Figure 2.5.: Schematic illustration of the trickling filter, modelled as a series of $n_{TF,CSTR}$ CSTRs, focus on a single CSTR ($CSTR_{TF,i}$); X stands for all particulate solids concentrations; S stands for all soluble matter concentrations

$$f_{V,TF,in} = f_{V,TF,out} = f_{V,TF,i,in} = f_{V,TF,i,out} \tag{2.28}$$

Where $f_{V,TF,out}$ stands for the volumetric flow out of the trickling filter, $f_{V,TF,i,in}$ and $f_{V,TF,i,out}$ stand for the volumetric flow in and out of CSTR number i.

Particulate matter travels unaffected through the trickling filter. To describe change in concentrations of particulate matter in each CSTR ($\frac{\mathrm{d}X_{TF,i}}{\mathrm{d}t}$), differential equations like equation 2.29 are used.

$$\frac{\mathrm{d}X_{TF,i}}{\mathrm{d}t} = \frac{1}{V_{TF,i}} * F_{V,in} * (X_{TF,i,in} - X_{TF,i}) \tag{2.29}$$

Where $X_{TF,i,in}$ stands for the concentrations of particulate matter in the inflow of $CSTR_{TF,i}$, for the first CSTR, this is equal to $X_{TF,in}$, for every other CSTR this is equal to the concentrations in the previous one ($CSTR_{TF,i-1}$).

$V_{TF,i}$ stands for the volume of a single CSTR and is calculated based on the cross-sectional area of the trickling filter ($A_{TF,CS}$), its height (h_{TF}), the number of CSTRs ($n_{TF,CSTR}$), and the void fraction of the medium (ε_{TF}), see equation 2.30.

$$V_{TF,i} = A_{TF,CS} * \frac{h_{TF}}{n_{TF,CSTR}} * \varepsilon_{TF} \tag{2.30}$$

The rate at which ammonia-N reacts to nitrate-N in each CSTR $r_{TAN,i}$, depends on the concentration of ammonia-N in that CSTR ($[TAN]_{TF,i}$). According to the model of Nijhof (1995), this reaction rate follows 0 and 1/2 order dynamics. His model depends on three parameters, a_{rTAN}, b_{rTAN} and c_{rTAN}. Nijhof (1995) estimated that a_{rTAN} depends on the hydraulic loading of the trickling filter (equation 2.31), b_{rTAN} he estimated to be equal to 0.2 $g/m^2/d$, and c_{rTAN} is the 0 order dynamics reaction rate of ammonia-N, assuming ideal aeration this has been estimated to be equal to 0.7 $g/m^2/d$.

$$a_{rTAN} = 7.81 * 10^{-4} * \frac{f_{V,TF,in}}{A_{TF,CS}} \tag{2.31}$$

According to Nijhof (1995) the reaction follows the 1/2 order dynamics at low ammonia-N concentrations ($[TAN] < (a_{rTAN}/b_{rTAN})^2$), at higher concentrations it follows the 0 order dynamics (equation 2.32).

$$r_{TAN,i} = \begin{cases} a_{rTAN} * \sqrt{[TAN]_{TF,i}} - b_{rTAN} & \text{if } [TAN]_{TF,i} < (\frac{a_{rTAN}}{b_{rTAN}})^2 \\ c & \text{otherwise} \end{cases} \tag{2.32}$$

The change of ammonia-N concentration in each CSTR ($\frac{\mathrm{d}[TAN]_{TF,i}}{\mathrm{d}t}$) is then calculated by differential equation 2.33.

$$\frac{\mathrm{d}[TAN]_{TF,i}}{\mathrm{d}t} = \frac{1}{V_i} * F_{V,in} * ([TAN]_{TF,i,in} - [TAN]_{TF,i} - r_{TAN,i} * A_{MS,i}) \tag{2.33}$$

Where $A_{MS,i}$ stands for the medium surface area in CSTR number i. Due to the one-to-one proportion, the change in nitrate-N ($\frac{\mathrm{d}[NO_3]_{TF,i}}{\mathrm{d}t}$) is the opposite of the change in ammonia-N (equation 2.34).

$$\frac{\mathrm{d}[NO_3]_{TF,i}}{\mathrm{d}t} = -\frac{\mathrm{d}[TAN]_{TF,i}}{\mathrm{d}t} \tag{2.34}$$

The trickling filter model describes the dynamics of soluble substances and particulate matter flowing through the trickling filter. It estimates the reaction of ammonia to nitrate based on the model by Nijhof (1995).

2.6. Settling Tank (ST)

The retentate from the drum filter leaves the RAS loop and travels towards the hydroponic loop. This flow is relatively small and rich in solids. For the removal of solids from these small flows, settling tanks commonly used, which operate according to discrete particle settling principles (Tucker and Hargreaves, 2008).

Fernandes et al. (2014) found all particles in a RAS to be smaller than 300 μm. A particle with a density of 1.05 g/ml and a diameter of 300 μm has a settling velocity of 2.45 mm/s according to Stoke's law (equation 2.42). This gives a Reynolds number of 0.75, which shows that all particles settle in laminar flow and Stoke's law can be applied for settling tanks with very slow flow rates.

The model for the settling tank is based on mass balances and the solids removal efficiency of the settling tank. It is assumed no mixing occurs in the settling tank. Although settling tanks have high hydraulic retention time, the retention of soluble substances and particulate matter in the settling tank is ignored in this model. Further it is assumed, that no mixing occurs in the settling tank and that sludge and flow towards hydroponic system leave the settling tank continuously. A schematic illustration of the settling tank model can be seen in figure 2.6.

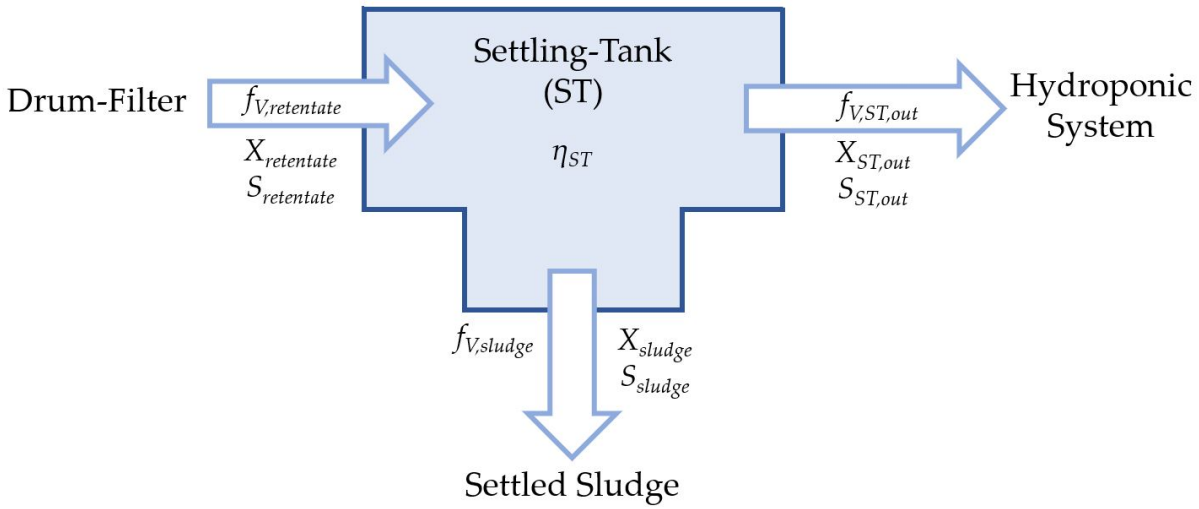

Figure 2.6.: Schematic illustration of the settling tank model; X stands for all particulate solids concentrations; S stands for all soluble matter concentrations

The volumetric flow out of the settling tank ($f_{V,ST,out}$) is calculated as difference of the retentate flow ($f_{V,retentate}$) and the settling flow ($f_{V,sludge}$), see equation 2.35.

$$f_{V,ST,out} = f_{V,retentate} - f_{V,settling} \tag{2.35}$$

To calculate the volumetric flow of the sludge, the concentration of particulate solids in the sludge (TSS_{sludge}) is used (equation 2.36). The TSS_{sludge} ranges around 75 mg/l (Tucker and Hargreaves, 2008).

$$f_{V,sludge} = \frac{f_{m,TSS,sludge}}{TSS_{sludge}} \tag{2.36}$$

Where $f_{m,TSS,sludge}$ is the total mass flow of particulate solids, which are removed by settling. The amount of settled particulate solids depends on the solids removal efficiency of the settling tank (η_{ST}) and the concentration of total suspended solids flowing into the settling tank ($TSS_{retentate}$), see equation 2.37. The solids removal efficiency of the settling tank is identified in section 2.6.1.

$$f_{m,TSS,sludge} = \eta_{ST} * TSS_{retentate} * f_{V,retentate} \tag{2.37}$$

The concentrations of particulate solids, which are removed by settling X_{sludge} and which leave the settling tank towards the hydroponic system $X_{settling_tank,out}$, are calculated based on the solids removal efficiency of the settling tank (equation 2.38 and 2.39).

$$X_{sludge} = \eta_{ST} * X_{retentate} * \frac{f_{V,retentate}}{f_{V,sludge}} \tag{2.38}$$

$$X_{ST,out} = (1 - \eta_{ST}) * X_{retentate} * \frac{f_{V,retentate}}{f_{V,ST,out}} \tag{2.39}$$

The mass of soluble matter in the sludge flow ($S_{sludge} * f_{V,sludge}$) and in the flow leaving the settling tank towards the hydroponic system ($S_{ST,out} * f_{V,ST,out}$) are equal to the concentrations of soluble matter entering the settling tank ($S_{retentate} * f_{V,retentate}$) (equation 2.40).

$$S_{sludge} * f_{V,sludge} = S_{ST,out} * f_{V,ST,out} = S_{ST,in} * f_{V,ST,in} \tag{2.40}$$

2.6.1. Solids Removal Efficiency

The removal efficiency of a settling tank depends on the size of particulate solids. It is calculated as shown in equation 2.41.

$$\eta_{ST,i} = \begin{cases} 1 & \text{if } \frac{v_{s_i}}{OR_{ST}} > 1 \\ \frac{v_{s_i}}{OR_{ST}} = \frac{A_{ST} * v_{s_i}}{f_{V,ST}} & \text{otherwise} \end{cases} \tag{2.41}$$

Where $\eta_{ST,i}$ is the settling tanks efficiency in removing particulate solids of size range i, v_{s_i} is the settling velocity of particulate solids of size range i and OR_{ST} is the settling tanks overflow rate which is calculated by dividing the volumetric flow through the settling tank ($f_{V,ST}$) by its area (A_{ST}). The efficiency can never exceed 1. The settling velocity per size range can be calculated by Stoke's law (equation 2.42).

$$v_{s,i} = \frac{g * (\rho_{faeces} - \rho_{water}) * \bar{d_i}^2}{18 * \mu_{water}} \tag{2.42}$$

Where g is acceleration due to gravity, ρ_{water} is the density of water, and μ_{water} is the dynamic viscosity of water. The total solids removal efficiency of the settling tank (η_{ST}) is than calculated as described in equation 2.43.

$$\eta_{ST} = \sum_i \frac{m_{particles,i}}{m_{particles}} * \eta_{ST,i} \tag{2.43}$$

Where $\frac{m_{particles,i}}{m_{particles}}$ stands for the mass fraction of particles in size range i. In section 2.4.1 it was shown that a power-law function and its β-value are appropriate to describe the partical size distribution in aquacultural waste water. In equation 2.44 it is shown how the mass fraction can be calculated from the β-value. For the validity of this normalization it is important, that the size ranges are arranged in such a way, that $\frac{\Delta d_i}{\bar{d_i}}$ is a constant, where

Δd_i stands for the difference between the maximum and the minimum particle size in size range i (Kavanaugh et al., 1980 cited in Patterson et al., 1999).

$$\frac{m_{particles,i}}{m_{particles}} = \frac{\rho_{faeces} * V_{particles,i}}{\rho_{faeces} * V_{particles}} = \bar{d_i}^{(4-\beta_{ST})} / \sum_i \bar{d_i}^{(4-\beta_{ST})} \tag{2.44}$$

Where $\frac{V_{particles,i}}{V_{particles}}$ is the volumetric fraction of particles in size range i and β_{ST} is the β-value of the particle size distribution in the settling tank inflow. The value for β_{ST} is estimated in section 3.4.

The model proposed for the settling tank estimates the efficiency of the settling tank based on the particle size distribution of particulate solids flowing into the settling tank. With this model, the volumetric flow to the hydroponic system and its soluble substances and particulate matter concentration can be estimated.

3. Parameter Estimation

In this chapter the estimation of model parameters is described, in the order shown in table 3.1. Parameters were estimated based on data found in literature. Equations shown in this chapter are used for parameter estimation and are not part of the model. It was tried to implement a wide range of datasets, to obtain a general model that accounts for uncertainties. When sufficient data was found, parameters were estimated by calibration. For calibration the least squares method was used to find a local minimum in the residuals between model and data-points. The Python™ least_squares function from the SciPy.optimize package was used for calibration. During calibration datasets were weight based on the amount of data-points, so that in total every dataset got the same importance.

Table 3.1.: Submodel parameters estimated in this chapter.

Section	Module	Estimated Parameters
3.1	Feeder	a_{DFR}, b_{DFR}, a_{growth}, b_{growth}
3.2	Fish	$\tau_{digestive}$, $\tau_{urinary}$, k_{uptake}, k_{faeces}, $k_{digestive \rightarrow urinal}$
3.3	Drum filter	η_{DF}, TSS_{cake}, $\Delta\beta_{DF}$
2.6	Settling tank	β_{ST}

For the trickling filter parameters estimated by Nijhof (1995) were used. For the fish tank no parameter estimation was required. Parameters estimated for the fish model are also validated.

Uncertainties of the calibrated parameters were calculated based on variance of datasets and residuals between model and data points. Parameter uncertainties are reported as standard deviations (σ). Model output uncertainties are estimated according to linear error propagation theory. To enable the use of uncertainties in the Python™ program, the Python™ uncertainties package was used and the Python™ source code had to be adapted.

3.1. Feeder

Both constants in the feeding ratio model (equation 2.1) were estimated by calibrating against data from literature. DeLong et al. (2009), J. Rakocy (1989) and (Wing-Keong and Romano, 2013) give scientific recommendations for the daily feeding ratio of tilapia depending on fish weight. The recommondations by a commercial feed supplier were also included (Aller Aqua, n.d.). Calibration results can be seen in figure 3.1 and table 3.2.

For calibrating the quadratic growth model used by the feeder, data on tilapia growth from several scientific papers was collected. Allaman et al. (2013) report growth data of four

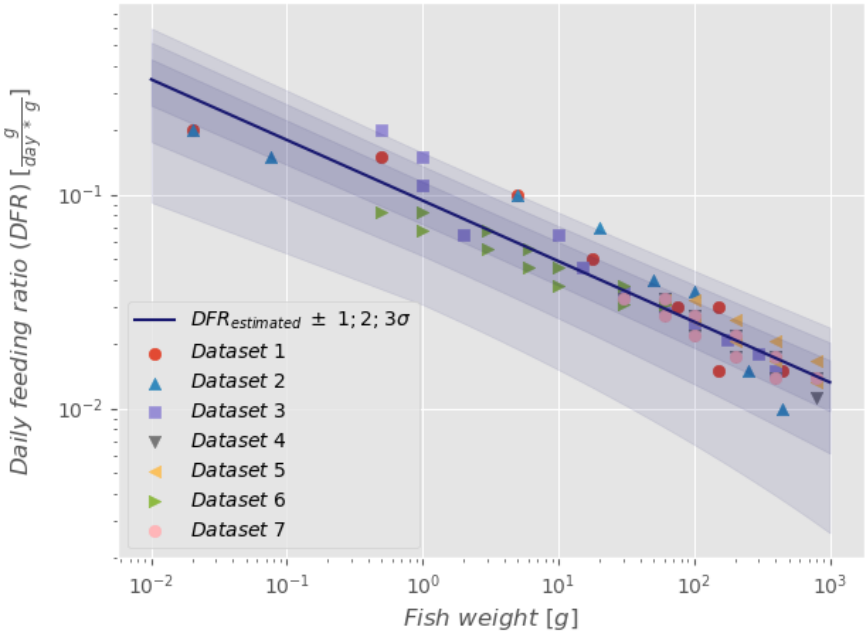

Figure 3.1.: Calibration of daily feeding ratio on log-log scale; Dataset 1, DeLong et al. (2009); Dataset 2, J. Rakocy (1989); Dataset 3, Wing-Keong and Romano (2013); Datasets 4, 5, 6, 7, daily feed ratio recommendations by feed supplier (Aller Aqua, n.d.); Shaded areas show parameter uncertainties; See table A.2 for full datasets

different tilapia strains cultivated in raceways. Amanico et al. (2014) and Gullian-Klanian and Arámburu-Adame (2013) report growth data of tilapia cultivated in RAS, Gullian-Klanian and Arámburu-Adame (2013) used three different stocking densities. (Santos et al., 2008) report growth data of two different tilapia strains cultivated in cages. Calibration results can be seen in figure 3.2 and table 3.2.

Table 3.2.: Results of parameter estimation for the feeder; parameters applied in equation 2.1 and 2.2.

Parameter	Estimation	Standard deviation (σ)	Covariance matrix
a_{DFR} $[\frac{1}{g*d}]$	0.0937	0.0021	$\begin{Bmatrix} 0.004 & -0.0002 \\ -0.0002 & 0.0001 \end{Bmatrix}$
b_{DFR} $[-]$	-0.2832	0.0111	
a_{growth} $[\frac{g}{d}]$	0.1997	0.1308	$\begin{Bmatrix} 1.7099 * 10^{-2} & -8.7370 * 10^{-5} \\ -8.7370 * 10^{-5} & 4.9630 * 10^{-7} \end{Bmatrix}$
b_{growth} $[\frac{g}{d^2}]$	0.0075	0.0002	

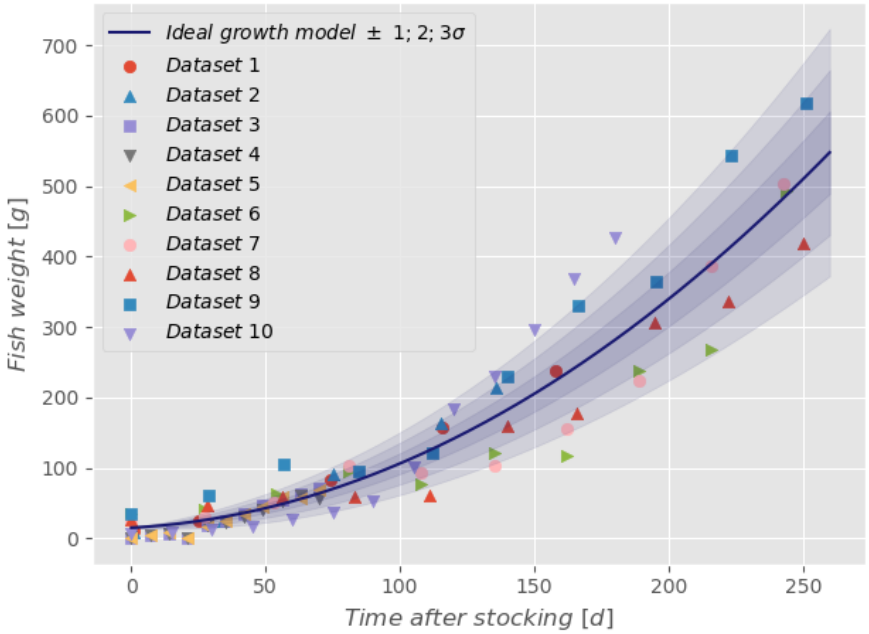

Figure 3.2.: Ideal growth model calibration; Datasets 1, 2, Santos et al. (2008); Datasets 3, 4, 5, Gullian-Klanian and Arámburu-Adame (2013); Datasets 6, 7, 8, 9, Allaman et al. (2013); Shaded areas show parameter uncertainties; See table A.3 for full datasets.

3.2. Fish

For the fish model both time constants, $\tau_{digestive}$ and $\tau_{urinary}$ had to be estimated to enable modelling of the excretion dynamics. Also the balances between uptake (k_{uptake}), faeces (k_{faeces}) and urine (k_{urine}) had to be defined. At the end of this section, the parameters estimated for the fish model are validated.

3.2.1. Digestive Tract and Urinal Tract Evacuation

In tilapia, evacuation of the digestive tract starts directly after feeding and decreases exponentially afterwards. This phenomenon has been found in several experiments, in which tilapia have been dissected at different times after feeding and their stomach content was either weighed or estimated by using a marker in the feed (Richter et al., 2003; Riche et al., 2004; Gómez-Pearanda and Clavijo-Restrepo, 2012). The dynamics of the digestive tract evacuation are expressed in the differential equation 2.4. The time constant $\tau_{digestive}$ was calibrated against stomach evacuation data. Results of the calibration can be seen in table 3.3 and figure 3.3.

Under all forms of soluble fish excreta, ammonia gets the most attention in aquacultural research, due to its high toxicity. Ammonia makes up 90% of all soluble N excretion, the rest is mostly urea (Timmons and Ebeling, 2013). With the nutrient balances given in table 2.3, the mass flow of soluble N excreta ($f_{m,\ N,\ urine}$) can be calculated by using equation 2.12.

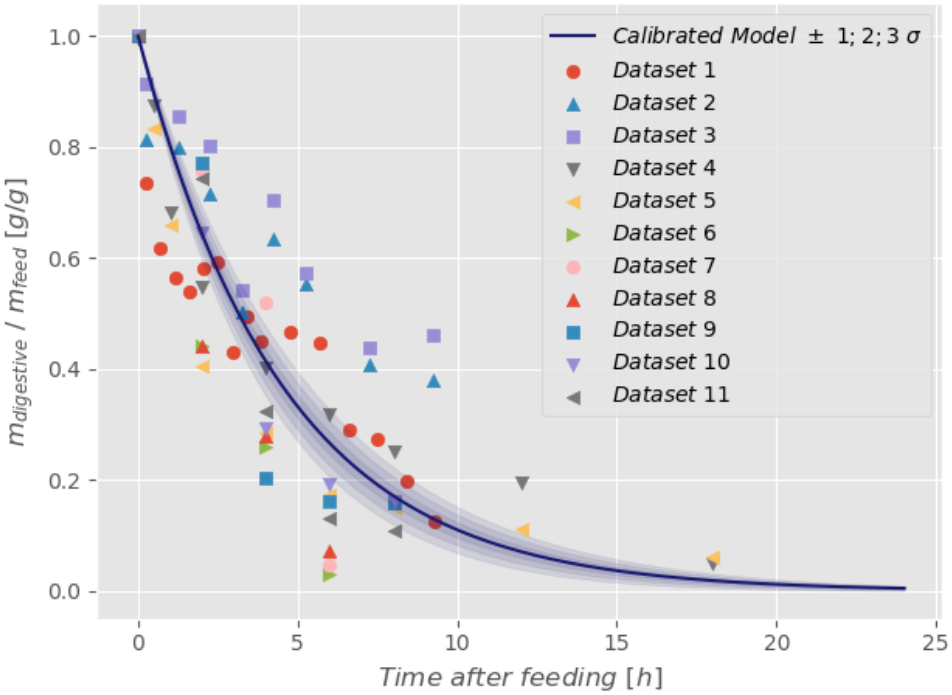

Figure 3.3.: Digestive tract evacuation calibration; Datasets 1, 2, 3, Richter et al. (2003); Datasets 4, 5, Riche et al. (2004); Datasets 6, 7, 8, 9, 10, 11, Gómez-Pearanda and Clavijo-Restrepo (2012); Shaded areas show parameter uncertainties; See table A.7 for full datasets.

Obirikorang et al. (2015) measured N concentrations in tilapia waste water, at different times after feeding, for four different diets. They report cumulative soluble N excretions relative to the amount of N taken up via feed, which show the diurnal dynamics in soluble N excretions. However, the dataset had to be modified to suit the calibration purpose and to go in line with the findings listed in table 2.3. All initial data points indicate that, at the time of feeding, ca. 2.5% of the consumed N, has already been excreted in soluble form. This was set to zero, by subtracting 2.5% from all data points. Afterwards the reported cumulative soluble N excretions come to a steady state at ca. 14.52% of N intake. According to the findings in table 2.3, this value should be 44.45%. To correct for this difference all data points were multiplied by a correction factor of 2.6.

The time constant $\tau_{urinary}$ is used to describe the dynamics of the urinal tracts evacuation time (equation 2.8). The modelled mass flow of soluble N excreta was calibrated against the ones found in literature, to estimate the time constants value. The results of the calibration are shown in table 3.3 and figure 3.4.

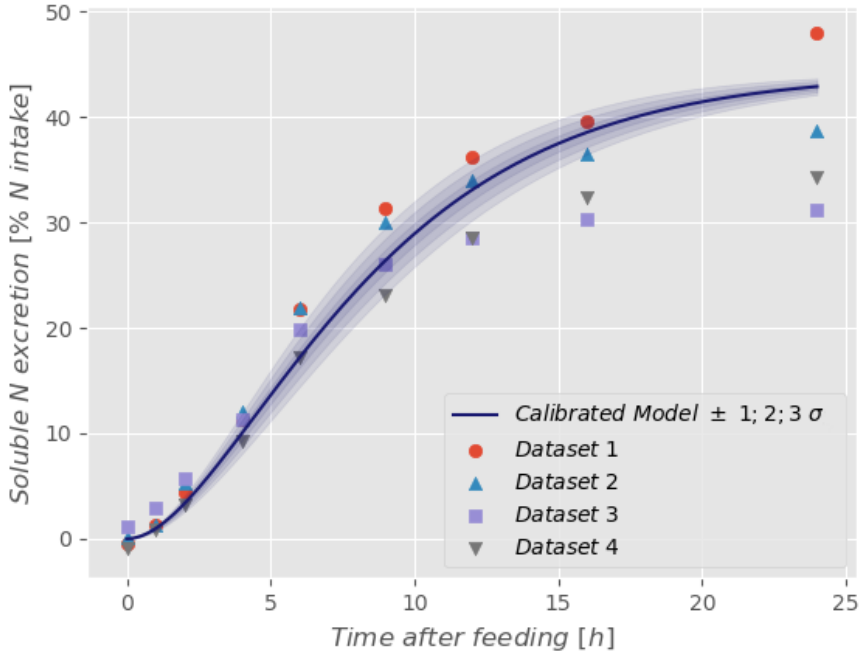

Figure 3.4.: Urinal tract evacuation calibration; Dataset 1, 2, 3, 4, Obirikorang et al. (2015); Shaded areas show parameter uncertainties; See table A.8 for full datasets.

Table 3.3.: Results of parameter estimation for evacuation of digestive and urinary tract; Both parameters were calibrated independently, so correlations are unknown.

Parameter	Estimation	Standard deviation (σ)
τ_{dig} $[h]$	4.55	0.26
τ_{uri} $[h]$	4.42	0.39

3.2.2. Balance between Uptake, Faeces and Urine

All consumed feed ends up eventually as uptake, faeces or urine as displayed in figure 2.1. The corresponding ratios therefore have to add up to 100%. First the faeces ratio (k_{faeces}) is defined, based on literature. Schneider et al. (2004) and Neto and Ostrensky (2015) report a ratio of consumed feed (DM) leaving the fish as solid excreta (DM), of 25% (±4%).

The uptake ratio (k_{uptake}) is estimated by calibration. The uptake flow results in growth (equation 2.7). The weight gain of the fish can be calculated as the cumulative integral of this mass flow (equation 3.1). To estimate k_{uptake}, the modelled fish growth was calibrated against fish growth data. The same data as in the calibration of the feeders quadratic growth model was used (section 3.1). The results of this calibration are shown in table 3.4 and figure 3.5.

$$m_{fish}(t) = \int_0^t f_{m,uptake}(t)\mathrm{d}t \tag{3.1}$$

The remaining ratio, to close the mass balance, is the ratio of digestive tract content that goes to the urinal tract and leaves the fish eventually as soluble excreta ($k_{digestive \to urinal}$). It is calculated by closing the balance, with the values found for k_{faeces} and k_{uptake}. All ratios are shown in table 3.4.

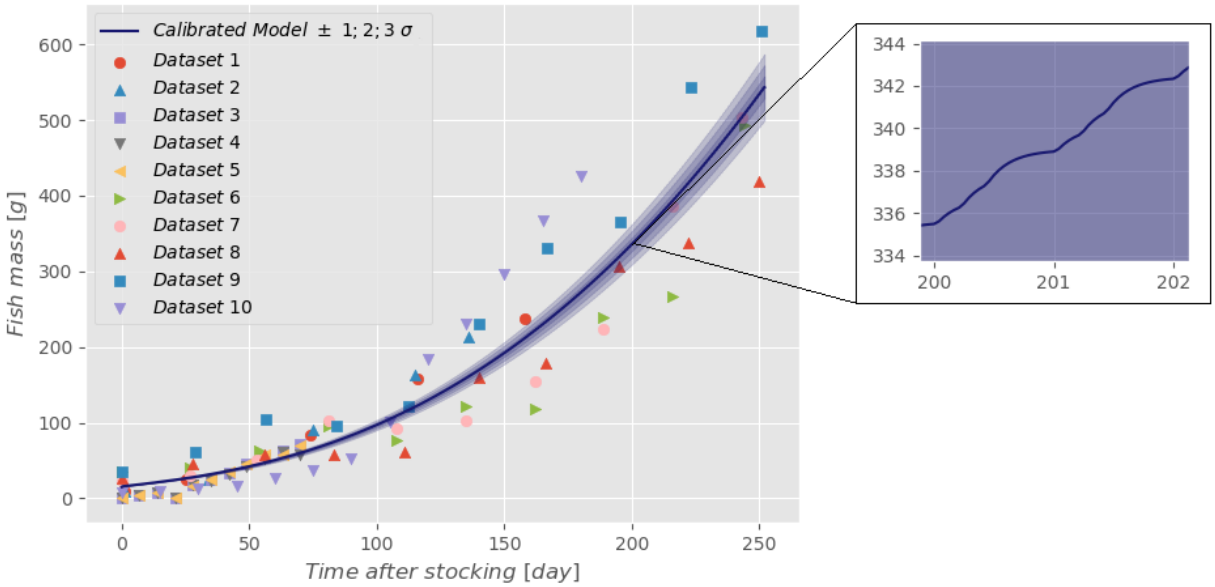

Figure 3.5.: Uptake calibration; Datasets 1, 2, Santos et al. (2008); Datasets 3, 4, 5, Gullian-Klanian and Arámburu-Adame (2013); Datasets 6, 7, 8, 9, Allaman et al. (2013); Shaded areas show parameter uncertainties; Zoom in shows that the uptake follows the pattern of the daily feeding schedule (7:00, 12:00 and 17:00); See appendix for full datasets

Table 3.4.: Ratio balance of flows out of the digestive tract; parameters applied in equation 2.7

Parameter	Value	Standard Deviation (σ)
k_{uptake} [−]	0.195	0.005
k_{faeces} [−]	0.25	0.04
$k_{digestive \to urinal}$ [−]	0.55	0.04

Faeces ratio based on Schneider et al. (2004); Uptake ratio estimated through calibration (see figure 3.5); Digestive to urinal tract ratio calculated as difference to close the mass balance; Standard deviation of $k_{digestive \to urinal}$ is calculated by linear uncertainties propagation; Correlation between single parameters is unknown.

3.2.3. Model Validation

To verify the excretion model and the parameter estimation results for $\tau_{digestive}$ and $\tau_{urinary}$, the soluble N excretion was cross validated with data reported by Obirikorang et al. (2017). They give mass flows of soluble N excreta for three different feed types, and use similar methods as Obirikorang et al. (2015), who's results were used for the estimation of $\tau_{urinary}$ (section 3.2.1). Since similar methods were used, the validation data was also corrected by a factor of 2.6. Validation shows that 70% of the data points lay within a 3 σ range. Figure 3.6 shows that the modelled soluble N excretion follows the same dynamics as the one reported by Obirikorang et al. (2017).

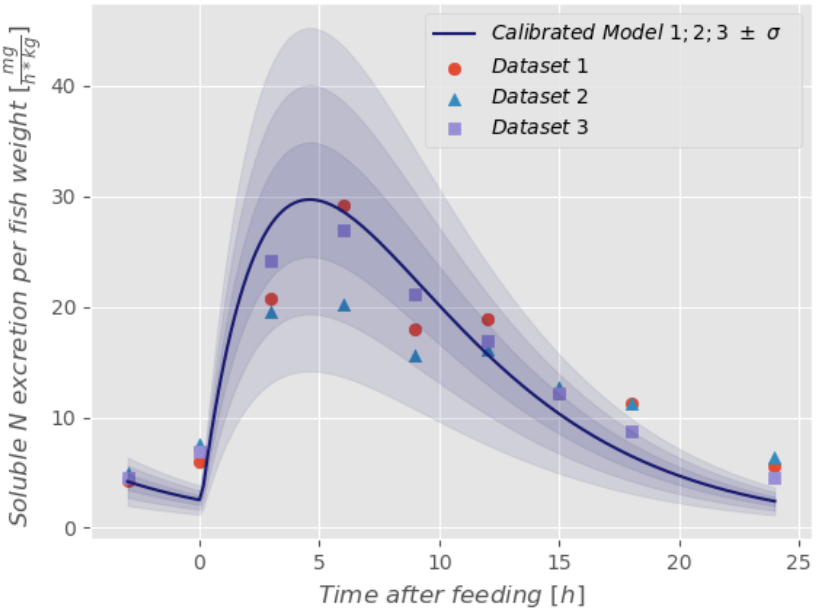

Figure 3.6.: Validation of modelled soluble N excretion; Datasets 1,2,3, Obirikorang et al. (2017); Shaded areas show model uncertainties; See appendix for full dataset.

The estimated parameter k_{uptake} gives the ratio of feed (DM), that is turned into fish body mass (DM). It quantifies how effective the fish takes up feed. To verify the parameter estimation result one can compare it to the feed conversion ratio (FCR), a parameter commonly used in aquaculture for describing uptake efficiency. It tells how many kg feed (wet weight) are needed, to produce one kg (wet weight) of fish. Taking the inverse of the found k_{uptake} value and correcting it for the dry mass content of tilapia and fish feed, one gets a value comparable to the FCR of 1.7 ($\pm$0.1). Commonly the FCR of tilapia lies in the range of 1.4 to 1.8 (DeLong et al., 2009).

3.3. Drum Filter

3.3.1. Solids Removal Efficiency

The rate in which a micro-screen drum-filter removes solids from a RAS water-stream depends on the concentration of all particulate solids in the inflow, which is equal to the concentration of particulate solids in the fish-tank (TSS_{FT}). A higher concentration results in a higher removal efficiency (Kelly et al., 1997). Summerfelt et al. (2001) (cited in Timmons and Ebeling, 2013) collected data on the removal efficiency of four different micro-screen filter, with screen aperture sizes ranging from 60-90 µ m, and inflow particulate solids concentrations ranging from 0.7 to 52.9 mg/l.

Based on the trend in the data, a logistic function was constructed, that describes the solids removal efficiency (η_{DF}) depending on the solids concentration in the inflow and three unknown constants (a_{DF}, b_{DF}, c_{DF}), where c_{DF} stands for the limit, which must be lower or equal to 100% (equation 3.2). Results of the calibration can be seen in table 3.5 and figure 3.7. Verification of the results is given by the fact, that even in a range of three standard deviations, the estimated drum filter efficiency doesn't exceed the limit of 100%.

$$\eta_{DF}(TSS_{FT}) = \frac{a_{DF}}{1 + e^{-b_{DF} * (TSS_{FT} - c_{DF})}} \; ; \; \lim_{TSS_{in} \to \infty} \eta_{DF}(TSS_{FT}) \leq 100\% \tag{3.2}$$

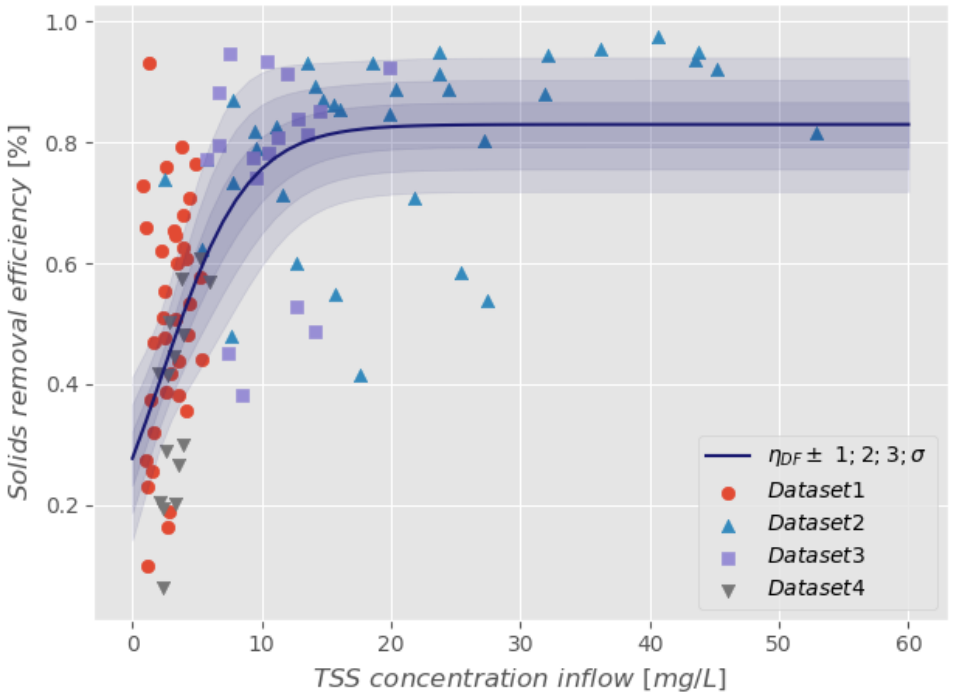

Figure 3.7.: Drum-filter efficiency calibration; Dataset 1, 2, 3, 4, Summerfelt (2001) cited in Timmons and Ebeling (2013); Shaded areas show parameter uncertainties; See appendix for full datasets

Table 3.5.: Results of parameter estimation for drum filter efficiency; parameters applied in equation 3.2.

Parameter	Estimation	Standard deviation (σ)	Covariance matrix
a_{DF} $[-]$	0.83	0.04	$\begin{Bmatrix} 0.0014 & -0.0017 & 0.0087 \\ -0.0017 & 0.006 & 0.004 \\ 0.0087 & 0.004 & 0.262 \end{Bmatrix}$
b_{DF} $[L/mg]$	0.30	0.08	
c_{DF} $[mg/L]$	2.3	0.5	

3.3.2. TSS Concentration in Cake

To calculate the volumetric cake flow of the drum filter, the concentration of TSS in the cake needs to be known (equation 2.18). Little is known about the composition of drum filter cakes. The only related data found says that the TSS concentration in the retentate ranges from 1 to 20 g/l (Tucker and Hargreaves, 2008). With the assumption that no particulate matter enters the drum-filter via the backwash, TSS_{cake} can be calculated as shown in equation (3.3).

$$TSS_{cake} = \frac{f_{m,TSS,cake}}{f_{V,cake}} = \frac{f_{m,TSS,cake}}{f_{m,TSS,cake}/TSS_{retentate} - f_{V,backwash}} \tag{3.3}$$

Reformulation of equation 3.3, setting $f_{V,backwash}$ to 1% of the drum filter inflow and replacing $f_{m,TSS,cake}$ by equation 2.19 yields equation 3.4.

$$TSS_{cake} = ((TSS_{retentate})^{-1} - \frac{f_{V,backwash}}{f_{m,TSS,cake}})^{-1} = ((TSS_{retentate})^{-1} - \frac{0.01}{\eta_{DF} * TSS_{FT}})^{-1} \tag{3.4}$$

In section 3.3.1 it was shown that a TSS concentration of 30 mg/l gives a removal efficiency of 83%, assuming this corresponds to the minimum $TSS_{retentate}$ concentration reported by Tucker and Hargreaves (2008) (1 g/l), TSS_{cake} is estimated to be equal to 3.26 g/l.

3.3.3. Particle Size Distribution

As shown in section 2.4.1 a power law function and its β-value can be used to characterise particle size distribution in RAS. Further it was proposed to describe a drum filters performance by an increase of the β-value (2.26). Stokic (2012) collected data on particle size distribution in tilapia RAS, measurements were taken before and after a drum filter, results are given as total weight per size class. To calculate the particle count, it is assumed that all particles are of spherical shape, with the size class' mean value as diameter (equation 3.5).

$$N_i = \frac{TSS_i * \frac{1}{\rho_{faeces}}}{\frac{3}{4} * \pi * \bar{d}_i} \tag{3.5}$$

Where TSS_i stands for the concentration of particles in size class i, and ρ_{faeces} for the density of faeces. Tilapia faeces have a density of 1.05 g/ml (Timmons and Ebeling, 2013).

The data from Stokic (2012) was used to estimate the β-value before and after micro-screen filtration. The parameter estimation results are shown table 3.6 and figure 3.8. It can be seen that the micro-screen filtration causes the β-value to increase by 0.19 ($\pm$0.21).

Table 3.6.: Results of parameter estimation for particle size distribution.

Parameter	Estimation	Standard deviation (σ)
$\beta_{before\ DF}$	3.35	0.17
$\beta_{after\ DF}$	3.54	0.12
$\Delta\beta_{DF}$	0.19	0.21

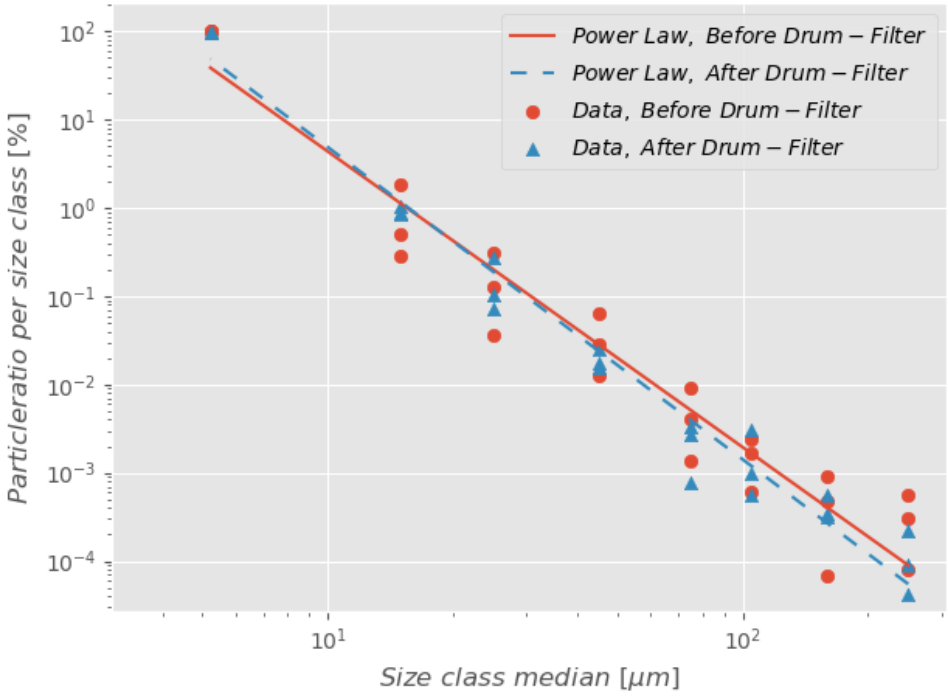

Figure 3.8.: Particle size distribution calibration; Presented on a log-log scale; Data from Stokic (2012); See appendix for full dataset.

3.4. Settling Tank

In section 2.6.1 it was shown that the solids removal efficiency of the settling tank depends on the particle size distribution in the settling tank inflow (equation 2.43).

All particles flowing into the settling-tank were previously filtered out by the drum filter. In the course of the filtration, high forces and turbulences were applied to the particles by the pressurised backwash flow. Little is known about the effect of pressurised backwashing on the particle size distribution and no reference reporting particle size distributions in a

settling tank was found. It is assumed that the particle size distribution in a settling tank also can be described by a power law function and its β-value (see section 2.4.1). Bergheim et al. (1998) report on the performance of a settling-tank, used to treat the backwash and retentate flow of a micro-screen filter in a salmon RAS. Salmon faeces are, with a density of 1.15 mg/l (Patterson et al., 2003), slightly denser than tilapia faeces.

Bergheim et al. (1998) found solids removal efficiencies ranging from $75 - 90\%$. The reported overflow rates vary between 0.02 and 0.2 m/h. Equations 2.41 to 2.44 and the particle size ranges proposed by Patterson et al. (1999) were used to calculate the efficiency of the settling tank described by Bergheim et al. (1998). Assuming that the lowest overflow rate corresponds to the highest removal efficiency, and vice versa, it was found numerically, that a β_{ST}-value of 3.35 gives the best fit to the efficiencies reported by Bergheim et al. (1998).

Further it is assumed that the β_{ST}-value has an uncertainty in the same range as the β-value uncertainties estimated in section 2.4.1. A mean of these uncertainties is assigned to it ($\beta_{ST} = 3.35$ (± 0.15)).

Afterwards the particle size distribution of the flow entering the settling tank can be calculated with equation 2.44. And the solids removal efficiency depending on the overflow rate can be calculated with equation 2.43. Settling tanks operate with small overflow rates, Bergheim et al. (1998) report overflow rates ranging from 0.02 to 0.2 m/h. The corresponding estimated solids removal efficiency of the settling tank is shown in figure 3.9.

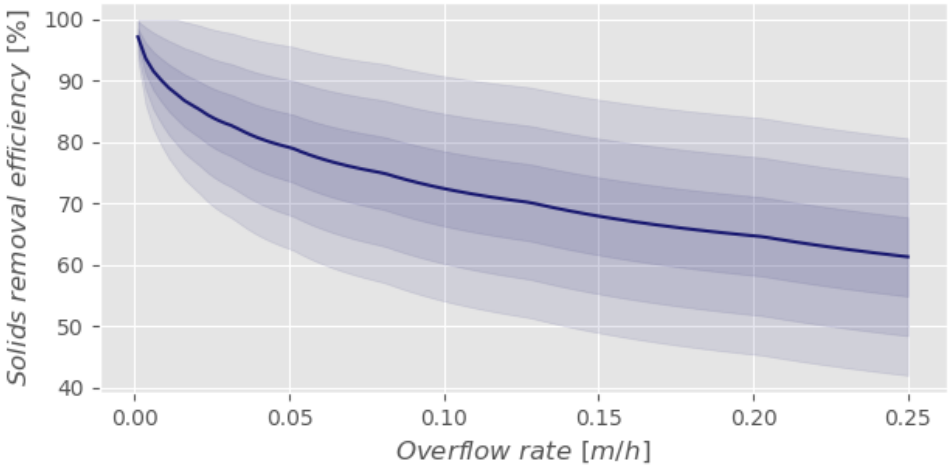

Figure 3.9.: Solids (tilapia faeces) removal efficiency of the settling tank depending on overflow rate with a particle size ditribution β_{ST}-value of 3.35 (± 0.15); Shaded areas show parameter uncertainties.

4. Simulation Results and Discussion

In this chapter simulation results are presented and discussed. The feeder and fish modules were evaluated by a short representative simulation of feeder and fish over four days with a total fish mass of 1 kg. All other modules are effected by the recirculating nature of the system, therefore a whole system simulation was run. The modelled system was oriented on Monsees et al. (2017), who reported data on a system with a setup comparable to the one modelled in this study. Model outputs were compared to this data.

In the fish simulation parameter uncertainties were included. Model uncertainties were predicted according to linear error propagation theory. To enable the use of uncertainties in the Python™ program, the Python™ uncertainties package was used and the Python™ source code had to be adapted. Model uncertainties of the fish module were analysed afterwards.

4.1. Feeder and Fish Simulation

In this section results of the feeder and fish model are presented. A representative simulation over four days was run with 10 fish, 100 g each. Feed was given on the first three days at 7:00, 12:00 and 17:00. Apart from the feeder parameters, all parameter uncertainties were included in the simulation. Feeder uncertainties are assumed to exist only between different automatic feeder settings. With a fixed automatic feeder setting, these uncertainties should not occur. It is assumed that an aquaponic system has a fixed automatic feeder setting so that the feeder parameter uncertainties do not occur. The effect of all relevant parameter uncertainties on model uncertainties is analysed at the end of this section.

Figure 4.1 shows the mass flow of feed, uptake, faeces and urine. The feed flow gives relatively high pulses at feeding times, 7:00, 12:00, and 17:00 on the first three days of simulation. Uptake, faeces and urine flows stretch the pulse input out over a longer timespan. The magnitudes of these flows are three decimals smaller than the one of the feed flow. Uptake and faeces flow are almost identical. Due to a simulation time of 15 minutes, both peak 15 minutes after each feeding. The urine flow peaks 2.75 hours after each feeding. Urine excretion builds up throughout the day and is the highest after the last feeding of the day. After one day of starvation all flows decreased to zero.

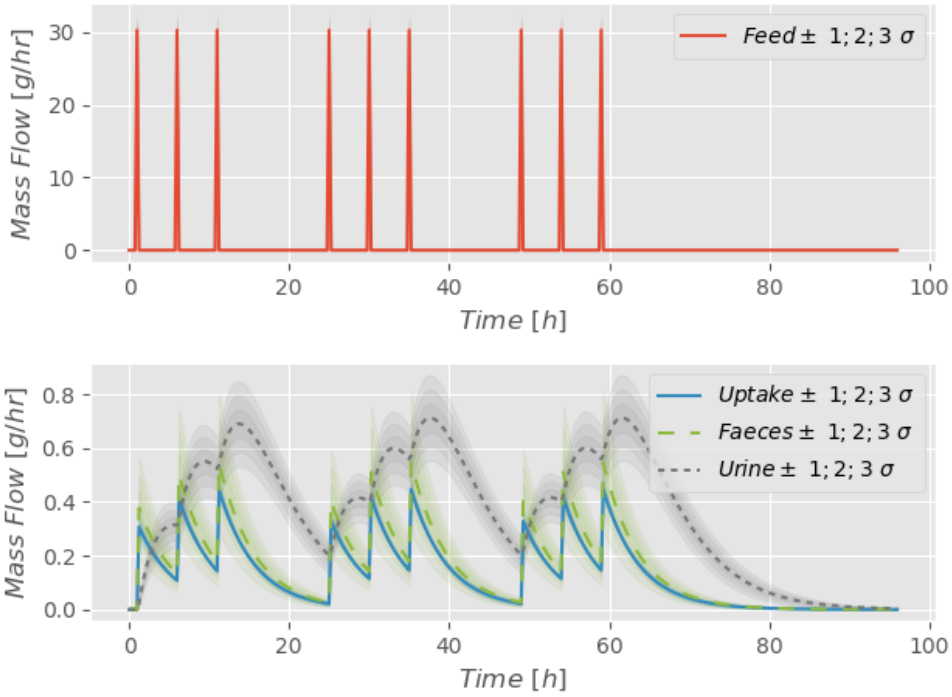

Figure 4.1.: Mass flow of feed, uptake, faeces and urine during a four-day simulation of 10 fish, 100 g each; Shaded areas represent model uncertainties.

Figure 4.2 illustrates the cumulative masses flowing into the fishes intestines and leaving them. Inflows are positive and outflows are negative. From the step increase in cumulative feed flow, one can see the impulse like feed distribution at feeding times. After four days the fish consumed 68 (± 2) g of feed and gained 13.0 (± 0.1) g of dry weight. Total excreta after the simulation are 16 (± 3) g of faeces and 35 (± 3) g of urine. Subtracting the cumulative mass of dry matter uptake, faeces and urine from the cumulative mass of feed consumed by the fish, gives a result of 4 g. This is a slight error in the model, the mass entering the fish intestines should be equal to the mass leaving them. It is assumed this error arises from the incapability of the model to accurately represent an impulse. However, the error is only 6% of the total mass of feed consumed by the fish and is therefore neglected in following simulations.

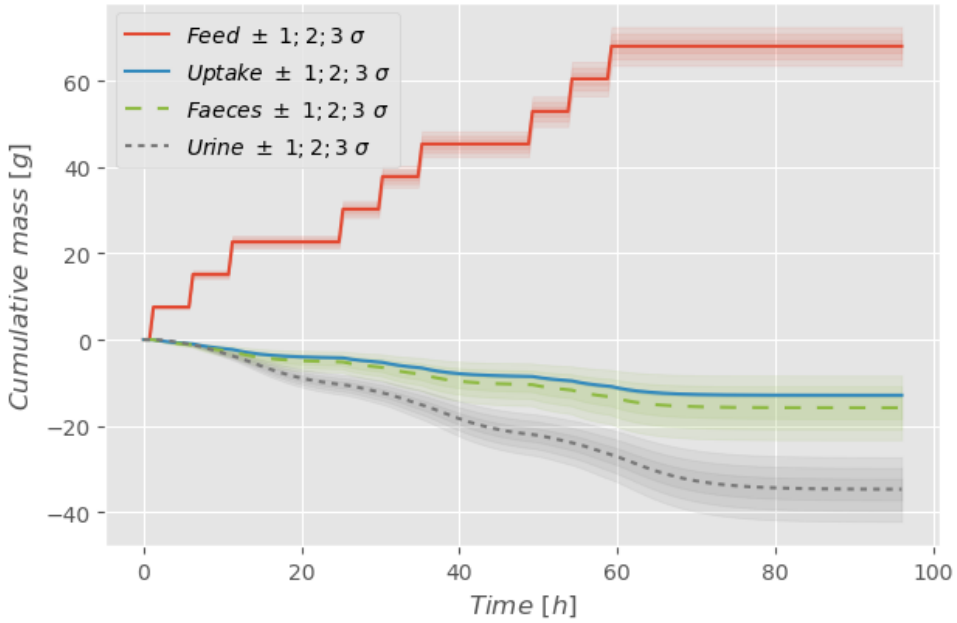

Figure 4.2.: Cumulative masses entering (positive) and leaving (negative) digestive and urinal tract during a four-day simulation of 10 fish, 100 g each.

In figure 4.3 the cumulative excretion of C, N, P, K, Ca, Mg and Na are demonstrated. For each nutrient soluble and particulate excreta are shown. With 13.8 ($\pm$0.3) g of soluble excreta and 4.13 ($\pm$0.09) g of particulate excreta at the end of the four day simulation, C is by far the biggest excretion component. Second in total size is N, with 1.5 ($\pm$0.2) g of soluble excreta and 0.38 ($\pm$0.06) g of particulate excreta. All other nutrient excreta are less than 1 g. Apart from P, all nutrients are excreted more in soluble form than in particulate. Soluble P excretion and particulate K excretion are almost zero, 0.03 ($\pm$0.02) g and 0.03 ($\pm$0.02) g respectively. For all nutrients but P, uncertainties of the soluble excreta are higher than those of particulate excreta.

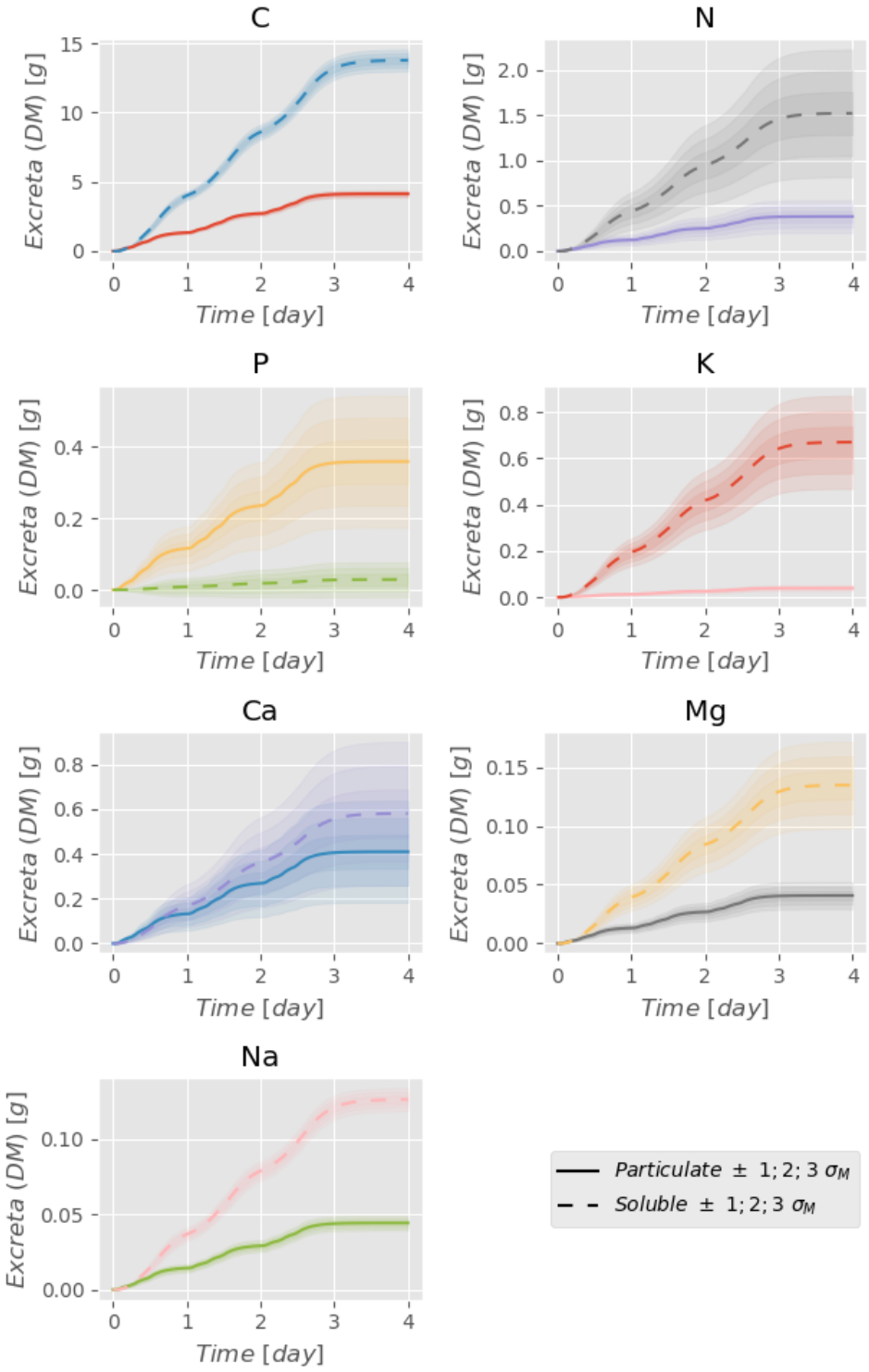

Figure 4.3.: Cumulative nutrient excreta in particulate and soluble form of 10 fish, 100 g each during a four day simulation.

4.1.1. Uncertainties Analysis

The effect of uncertainties in the parameters on the model outputs was determined using a one-at-a-time sensitivity analysis. The highest uncertainties in model outputs are expected shortly after feeding, when their change is maximal. Therefore model output uncertainties one hour after the last feeding (t=59 h) were compared. This was repeated for every parameter with uncertainties. Afterwards the origin of model output uncertainties could be determined, according to linear error propagation theory.

Figure 4.4 illustrates which parameter uncertainties lead to uncertainties in cumulative mass of feed, uptake, faeces and urine as well as in digestive and urinal tract mass content. Uncertainties in the cumulative feed mass arise completely from the feeds dry matter fraction uncertainty. The uncertainties in the cumulative mass taken up, come to 72.67% from the uptake fraction uncertainty, to 20.09% from the digestive tracts time constant uncertainty and to 6.47% from the fishes dry matter fraction uncertainty. The cumulative faeces and urine uncertainties originate almost completely from the uptake fraction uncertainty. Content mass of the digestive tract gets it uncertainty completely from the digestive tracts time constant uncertainty. Uncertainties in the content mass of the urinal tract arise to 50.70% from the urinal tracts time constant uncertainty and to 48.32% from the faeces fraction uncertainty.

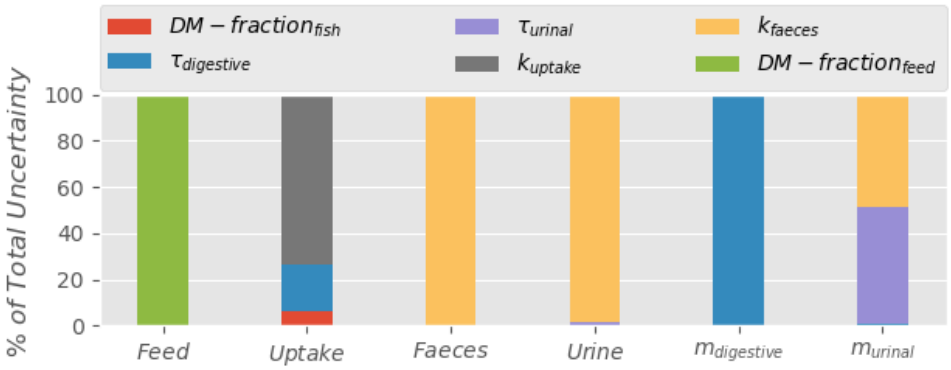

Figure 4.4.: Share of parameter uncertainties resulting in model output uncertainties at t=59 h in figure 4.1 and 4.2.

Figure 4.4 illustrates which parameter uncertainties lead to uncertainties in particulate and soluble excretion of the nutrients C, N, P, K, Ca, Mg and Na. Apart from soluble P excreta, all uncertainties in nutrient excretions originate to 70-99% from uncertainties in the corresponding nutrient fraction in the feed. The second biggest cause for uncertainties in nutrient excretions is uncertainties in the faeces fraction of the corresponding nutrient (0-26%). Uncertainties in soluble P excreta arise mainly from the uncertainty in the uptake fraction of P (66.48%).

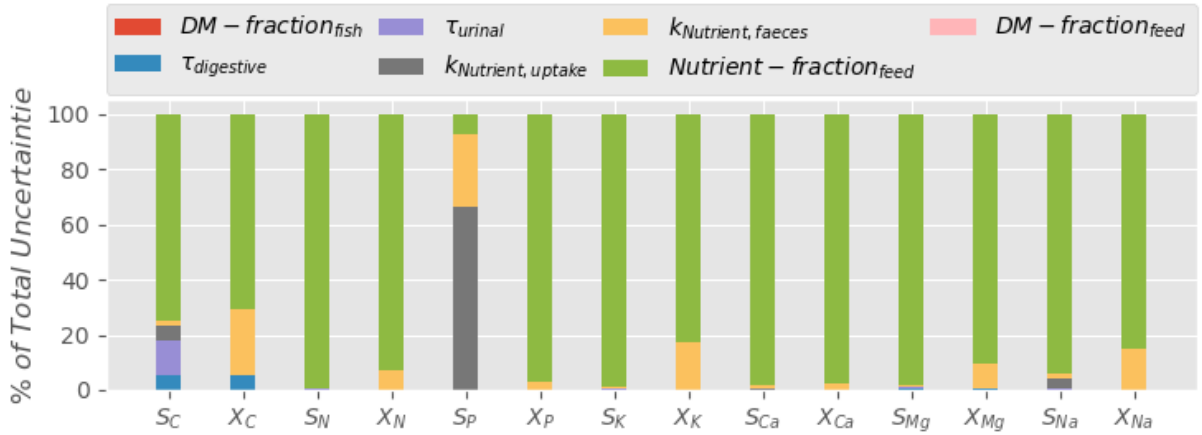

Figure 4.5.: Share of parameter uncertainties resulting in model output uncertainties at t=59 h in figure 4.3; X = particulate excreta; S=soluble excreta; $k_{Nutrient,uptake}$, $k_{Nutrient,faeces}$ and $Nutrient-fraction_{feed}$ stand for the fraction of the corresponding nutrient, that is taken up, excreted as faeces and present in the feed, respectively.

4.2. Full System Simulation

To analyse the concentrations of soluble substances and particulate matter in the fish tank and the performance of drum filter, trickling filter, and settling tank, a full system simulation was ran. It was aimed to simulate the system described by Monsees et al. (2017), to allow comparison between model outputs and measurements. The simulation was run for a time span of 5 month, with 1000 tilapia and an initial weight of 66.9 g per fish. Feeding was distributed each day at 7:00, 12:00 and 17:00. For initial nutrient concentrations and nutrient concentrations in fresh water entering the system, groundwater measurements from northern Germany, as reported by Kunkel et al. (2002), were used.

4.2.1. Feed and Fish Growth

Over the whole span of five months a total feed output of 478.44 kg (wet weight) is given by the model, which is 143.8 kg more than reported by Monsees et al. (2017). A final individual fish weight of 353.5 g is given by the model, whereas Monsees et al. (2017) reported 324.6 g. The overall feed conversion ratio in the model is therefore higher than the reported one (1.67 vs. 1.30). This implies that the modelled excretions are significantly higher than the ones observed by Monsees et al. (2017), what proves that the deterministic fish growth and feeder model are improper to model the referred system. All other models are heavily impacted by this.

4.2.2. Soluble Nutrient Concentrations in the Fish Tank

In figure 4.6 modelled concentrations of soluble nutrients in the fish tank can be seen. Apart from TAN, all nutrient concentrations increased in the run of the 5-month simulation. The

gain of all concentrations is decreasing over time, which indicates that all concentrations will reach a steady state eventually. TAN and P have the lowest concentrations of almost 0, which can be explained by the nitrification of TAN in the trickling filter and the bad solubility of P. The TAN concentration never exceeds 1.1 mg/L, which is only a third of the limit for tilapia (Timmons and Ebeling, 2013).

The final concentrations of soluble Mg and Na range at around 32 mg/L, K goes up to 111 mg/L, Ca reaches 160 mg/L, the highest concentration has NO_3 of about 223 mg/L, which is approaching the upper optimum NO_3 concentration for tilapia, of 300 mg/L (DeLong et al., 2009).

The zoom in shows how the diurnal excretion variations effect the concentration of TAN, it follows the pattern of the feeding schedule (feeding at 7:00, 12:00 and 17:00), with a diurnal peak-to-peak difference of 0.7 mg/L. Similar diurnal variances can be seen for the other nutrients. Overall this gives rather smooth lines, with relatively little diurnal variations in nutrient concentrations. This is an improvement compared to a previous model, where oscillations in nutrient concentrations had to be filtered out (Reyes Lastiri et al., 2018).

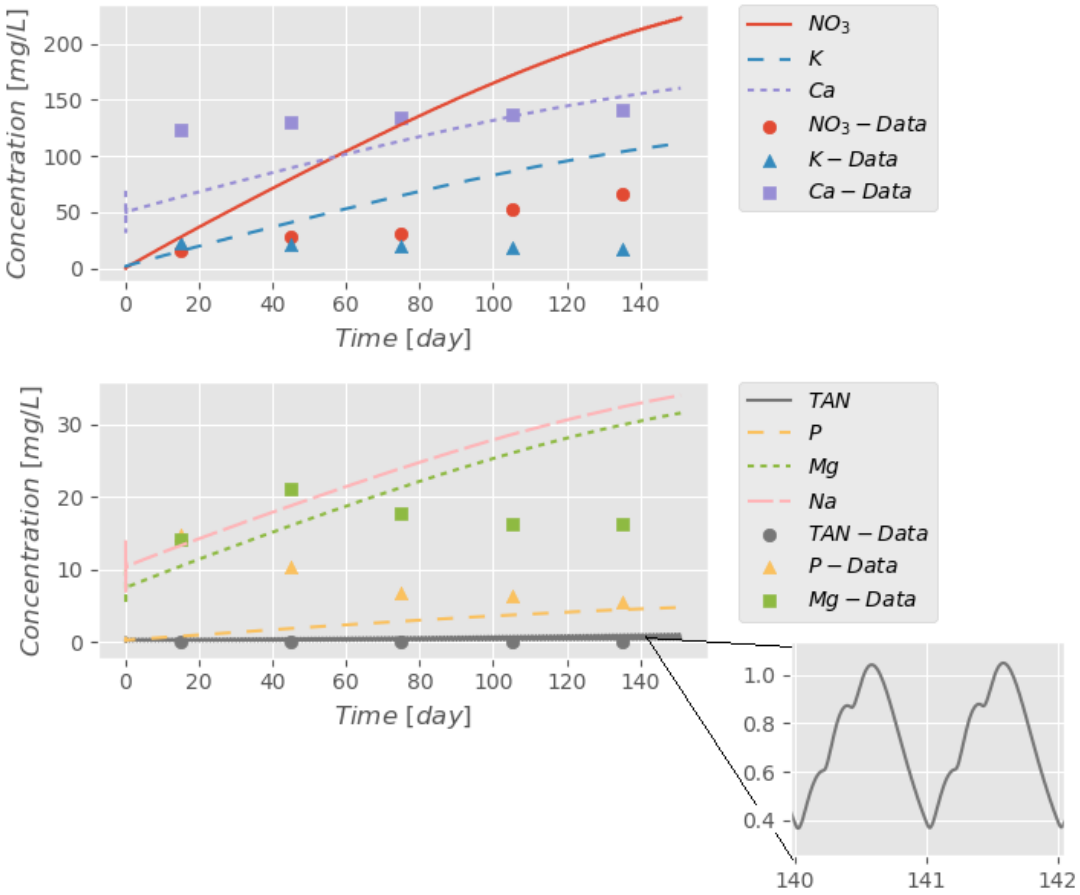

Figure 4.6.: Concentrations of soluble nutrients in the fishtank; Data from (Monsees et al., 2017) given for comparison; Zoom in on change in TAN concentration during two days.

In comparison to the values reported by Monsees et al. (2017), one can see that the TAN, P, Ca and Mg concentrations fall in the same range, the K and NO_3 concentrations are however overestimated. This could be explained by the higher excretion rates in the simulation (see section 4.2.1), or different nutrient concentrations in the initial and fresh water. Also, the model doesn't account for denitrification and the formation of biomass which can reduce the concentration of NO_3. However, the main reason for the difference might be the much lower water renewal rate in the modelled system, as explained in section 4.2.3. The deterministic model can not accurately estimate the nutrient concentrations in the system reported by Monsees et al. (2017).

4.2.3. TSS Concentration and Drum Filter Performance

The concentration of TSS oscillates more than the concentration of soluble nutrients (figure 4.7). This is due to the combination of the diurnal variation in TSS excretion and the constant TSS removal by the drum filter. Initially TSS concentrations in the fish tank range between 2.4 and 5.8 mg/L, over the simulation time this increases to a range of 3.8 to 19.8 mg/L. The concentration of TSS stays constantly below the limit for tilapia of 30 mg/L (Timmons and Ebeling, 2013). However, the high diurnal variations might cause stress for the fish.

To show the efficiency of the drum filter, TSS concentrations in the drum filter outflow are also shown in figure 4.7. Since the efficiency increases with an increasing TSS concentration coming in, the drum filter flattens out the variations in TSS concentrations. Concentrations in the drum filter outflow range initially between 1.4 and 2.4 mg/L and finally between 1.9 and 3.5 mg/L. The efficiency varies between 42-82%.

In comparison, Monsees et al. (2017) measured the TSS concentration to increase from 0.75 to 3.6 mg/L. A cause for the difference between the model and the data are the higher excretion rates in the simulation (see section 4.2.1), as well as the difference in water renewal, which is explained in the following paragraph.

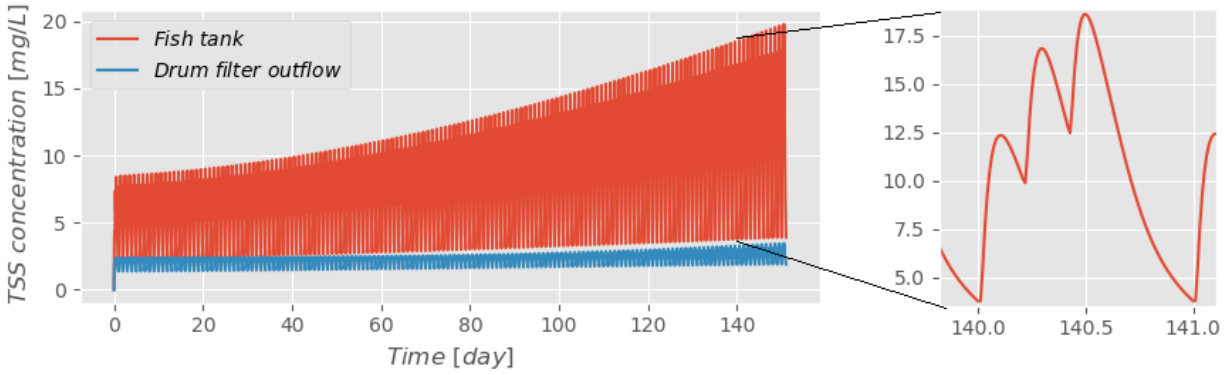

Figure 4.7.: Concentration of TSS in the fishtank; Zoom in on change in on variations during two days.

The volume of the cake is directly related to its TSS content; volumetric flows of cake,

retentate, and drum filter outflow therefore variate in the same pattern as the TSS concentration. The amount of water leaving the recirculating system as cake needs to be replaced by fresh water. For the modelled system this increases from an averaged 0.7 to 2.2% of the total system volume. Monsees et al. (2017) reports much higher water renewal percentages, increasing from 3.0 to 6.1% of the total system volume. This indicates that the volume of the cake is under estimated, what facilitates the accumulation of nutrients in the system water.

4.3. Trickling Filter Performance

In figure 4.6 one can see that almost no TAN accumulated in the fish tank. This shows that the trickling filter is very efficient in removing TAN. Figure 4.8 shows the concentration of TAN in each of the five consecutive CSTRs, which represent the trickling filter in total (see section 2.5). Diurnal varriations are very high, due to the variations in the inflow and high TAN reaction rates. In each consecutive CSTR the TAN concentration, as well as its diurnal varriations, are decreased. On the final day of the simulation, TAN concentration in the first CSTR ranges from 0 to 0.27 mg/L and in the last one from 0 to 0.01 mg/L.

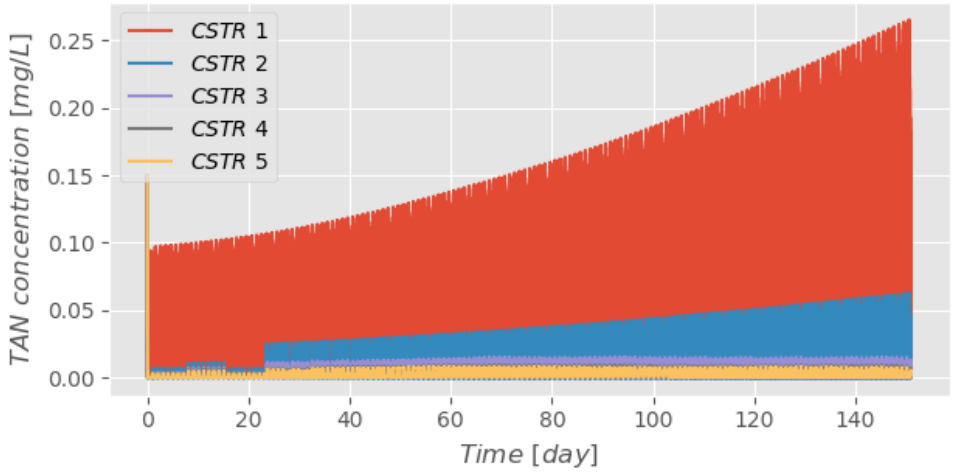

Figure 4.8.: Concentration of TAN in each of the 5 consecutive CSTRs, which represent the trickling filter in total (see section 2.5).

4.3.1. Settling Tank Outflow to Hydroponic System

The modelled concentration of soluble nutrients in the settling tank outflow is the same as in the fish tank (figure 4.6). This water is eventually going to the hydroponic system. The modelled concentrations are compared to concentrations required for optimal tomato growth as reported by Ross (1998) (figure 4.9).

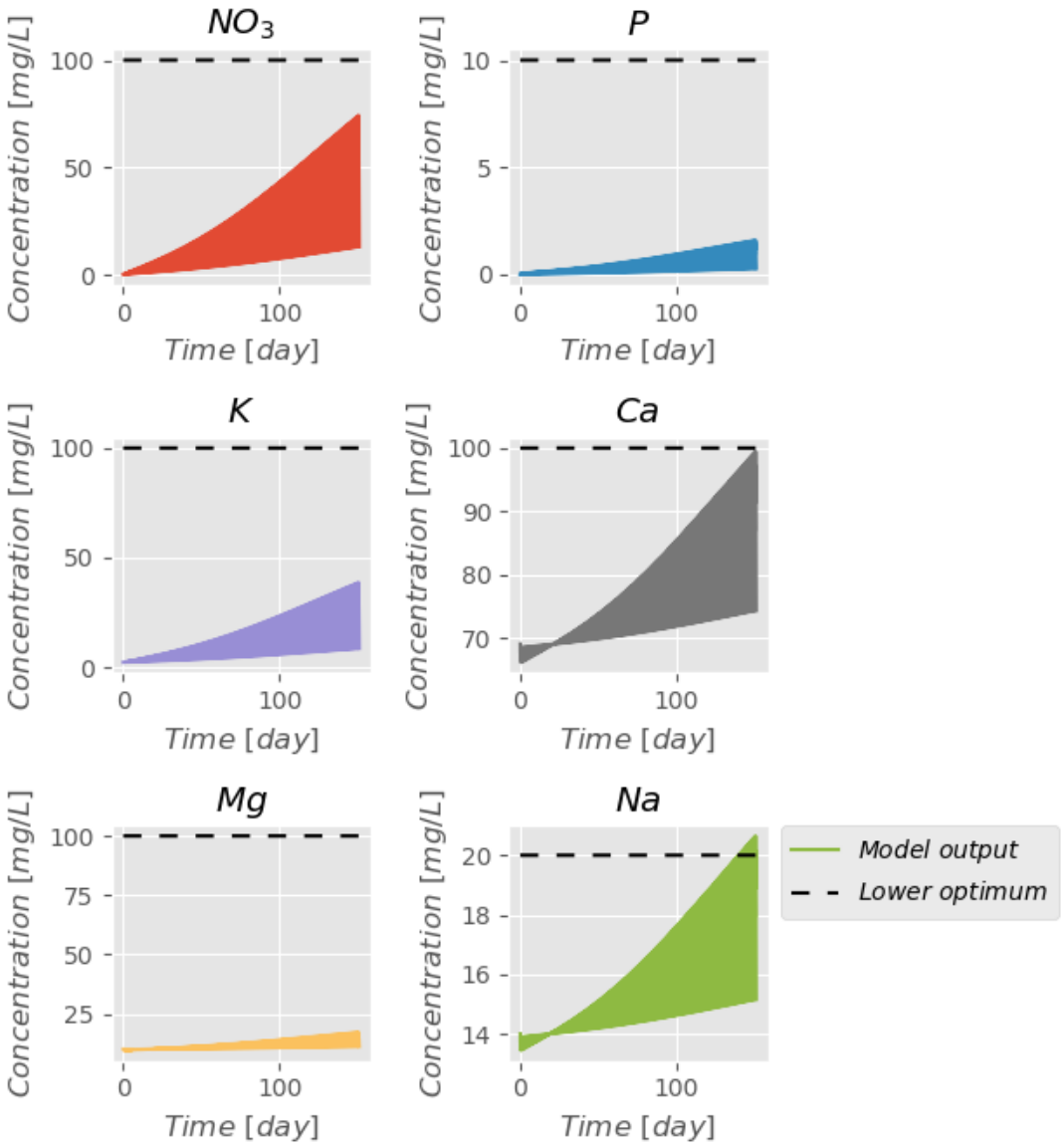

Figure 4.9.: Soluble nutrient concentrations in the settling tank outflow, compared to the lower optimum for tomato cultivation (as reported by Ross (1998)).

One can see that all nutrient concentrations oscillate. They oscillate in the same pattern as in the fish tank (figure 4.6). Ca and Na are the only two nutrients partly reaching the lower optimum for tomato cultivation. NO_3 is approaching it, with a maximum concentration of 75 mg/L. According to experimental aquaponic research, K is the nutrient lacking the most in fish waste water (Goddek, 2017; J. E. Rakocy, 2012). According to the model output Mg needs to be added the most, followed by K, then NO_3 and P. For Na it is important that the concentration doesn't exceed the upper optimum of 180 mg/L, which doesn't occur.

5. General Discussion and Conclusions

In this chapter general topics are discussed and conclusions with respect to the research questions are drawn per system module. In the end a general conclusions with recommendations for further improvement of the model are given.

5.1. Feeder

Automatic feeders distribute feed according to a feeding schedule and the expected demand of the fish. Programs for commercial automatic feeders are proprietary. The construction of a model which represents such a program was attempted. To allow general applicability, it was tried to estimate model parameters based on a wide range of data.

However, simulation of the system reported by Monsees et al. (2017) (section 4.2) showed that the deterministic feeder model was not able to represent the real system. Different feeding strategies can be used in RAS, a higher feed level results in faster growth. This however, usually comes at the expense of an increased feed conversion ratio. Economically speaking, lower feeding levels might make more sense, as they result in a lower growth rate as well as an improved feed conversion rate (Timmons and Ebeling, 2013). It seems that the data used for calibration, was taken from systems where high feeding levels were preferred. Monsees et al. (2017) on the other hand, appears to have used a feeding strategy with lower feeding levels.

The feeder is the main input of nutrients to the system and with its pulse shape it is the cause for diurnal variations in nutrient concentrations. To improve general applicability of the model, uncertainties of the feeder should be included in system simulations.

5.2. Fish

The fish model splits up the feed input into uptake, faeces, and urine. The impulsive input is spread over a longer time span. The resulting diurnal excretion variances have been investigated and implemented into the fish model. The modelled excretion rates mainly depend on the two time constants $\tau_{digestive}$ and $\tau_{urinary}$.

In order to get a generally applicable model, a wide range of data was used for the estimation of $\tau_{digestive}$. Riche et al. (2004) however, pointed out that no generally applicable model for the evacuation of a fish's digestive tract exists. This is due to the fact, that evacuation time is effected by different factors, such as feeding frequency, feed pellet size and feed digestibility. For a more precise model it would be necessary, to implement these factors. This however is difficult since most references do not mention all of the relevant factors. In the proposed model the effect of these factors is expressed by the uncertainty of

$\tau_{digestive}$. In the uncertainties analysis (section 4.1.1) it was shown that these uncertainties likely do not have a large impact on the model outputs.

Unlike assumed in previous models (Wik et al., 2009; Karimanziraa et al., 2016), experimental results indicate that excretion of soluble substances doesn't follow the same dynamics as the excretion of particulate matter (Obirikorang et al., 2015; Obirikorang et al., 2017). Soluble excreta are metabolised before excretion (Neto and Ostrensky, 2015), which supports the theory that soluble excretion will peak some time after feeding. To describe the rate of soluble excretion the parameter $\tau_{urinary}$ is used, which was calibrated against data reported by Obirikorang et al. (2015). Before calibration the data was adjusted, based on the experimental structure, two justifications were found for this:

1. Prior to both experiments, tilapia were starved for one day and the meal provided before the measurements was half as big as the meal on previous days. It is assumed that this led to a higher N uptake ratio and consequently lower N excretion ratios.

2. To measure changes in soluble N concentrations in the fish tank, recirculation was stopped during both experiments. Which means that ammonia concentrations build up through the experiment. It is known that fish can adapt their ammonia excretion to the ammonia concentration in the surrounding water. If the ammonia concentrations reaches a higher level than what the fish is acclimatised to, they can delay the excretion of soluble N (Chasiotis, n.d.).

The excretion rate of soluble N was used representative for all forms of soluble excreta. Most soluble N is excreted as ammonia via the gills, urine on the other hand has a different excretion path way and is excreted through the cloaca (D. Burton and M. Burton, 2017). It is therefore questionable how representative the excretion rate of soluble N is for the excretion rate of other soluble nutrients. However, no data on diurnal excretion rates of other soluble nutrients was found.

For the balance between uptake, faeces, and urine the constant parameters k_{uptake}, k_{faeces}, and k_{urine} have been estimated. As explained in section 5.1 the uptake ratio can be influenced by the feeding strategy. Also it is known, that young fish are more efficient at taking up feed (Timmons and Ebeling, 2013), which implies that the ratios are time variant. Implementing these factors into the model can yield more precise outputs.

For the balance between uptake, faeces and urine per nutrient, more data would be useful. To measure the composition of faeces particle, Patterson and Watts (2003) proposed to use scanning electron microscope examination. Such measurements for tilapia faeces at different growth stages would be highly beneficial.

In the simulation of the fish (section 4.1), linear error propagation theory was used to calculate model uncertainties. By the linearisation correlations are neglected, uncertainties might be overestimated. Also it was found that the uncertainties package used in Python™for linear error propagation could not be used for every simulation step, also the processing time of the model was highly increased by this package. A Monte Carlo approach with respect to parameter correlation might be more useful to estimate model uncertainties.

In conclusion the fish model creates diurnal excretion variations from the impulse feed input. Excretions of faeces peaks immediately after feeding, excretion of urine around 2.5

hours later, a daily maximum is reached after the last feeding of the day. To improve the accuracy of the fish model many factors can be added. However, parameter uncertainties could be used to account for these uncertainties. A Monte Carlo uncertainties analysis is recommended.

5.3. Fish Tank

The fish tank is modelled as continuously stirred tank, water mixing is done by fish movement and the flow through the fish tank. If this leads to perfect mixing is questionable. To account for the delay that might occur in mixing, a delay time was added to the system. For a more precise model, fluid dynamics in the fish tank would need to be implemented.

It was shown that diurnal excretion dynamics lead to oscillating soluble nutrient concentrations in the fish tank, with a peak shortly after feeding. In the simulated system the maximum peak-to-peak difference was 0.7 mg/L, increasing the fish density however would lead to stronger oscillation. The proposed model can be used to ensure that at no given time concentrations appropriate for fish cultivation are exceeded. Over the whole simulation time seen, the oscillation in nutrient concentrations becomes insignificantly small. This can be seen as an improve to a previous model, where ignoring of excretion dynamics lead to high oscillations in nutrient concentrations (Reyes Lastiri et al., 2018).

TSS concentrations in the fish tank vary in the same pattern. The magnitude of oscillation, however increases over time. This is due to the permanent removal of TSS by the drum filter. In the modelled system oscillation builds up to a peak-to-peak difference of 16.0 mg/L. In a system with higher fish density the oscillation would be higher. This can lead to a stressful environment for the fish.

In conclusion nutrient concentrations in the fish tank oscillate in the pattern of the excretion variations, the oscillations are however highly buffered by the dilution of the excreta. Due to delayed mixing in the fish tank, particulate nutrient concentrations peak an hour after feeding, soluble nutrient concentrations around 2.5 hours later. Modelling the exact fluid dynamics in the fish tank could increase the accuracy.

5.4. Drum Filter

In the drum filter model the amount of solids which are removed by the drum filter is calculated based on the estimated efficiency and the TSS concentration in the inflow. It was shown that TSS concentration oscillates, due to the excretion dynamics. This also leads to an oscillating drum filter performance. Shortly after feeding, when the TSS concentration peaks, also the amount of solids removed by the drum filter peaks.

The volume of the cake is calculated based on the TSS concentration in the cake. The cake TSS concentration is estimated with few data and big assumptions (see 3.3.2). Its liability is therefore questionable. More data on the composition of drum filter cakes is required to improve the model. For an aquaponic system the volumetric flow the cake is a key factor, since all nutrients are transported via that flow to the hydroponic system. Measurements

of TSS concentrations in the drum filter inflow and retentate would be highly beneficial to the model.

It was proposed in this study, to describe the drum filtration process by a change in particle size distribution. Estimation of particle size distributions before and after drum filtration indicated that there is a difference with small significance. Patterson et al. (1999) pointed out that the particle size distribution in RAS is heavily impacted by structural system differences. Evaluation of more particle size distribution data from different RAS is required to increase the significancie and to proove weather the same value holds for different systems. The particle size distribution is not implemented in the proposed model. To enable this, the particle size distribution of tilapia faeces and the effect of other system modules on the particle size distribution need be determined.

In conclusion the drum filter performance is highly affected by excretion variations. The Solids removal efficiency is maximal at high TSS concentrations. Especially at night, before the first feeding of the day TSS concentrations and drum filter efficiency are minimal. A decreased backwash flow at this time could decrease water usage and dilution of the retentate. The cake flow is a key factor for the aquaponic system, more data on its composition is highly required.

5.5. Trickling Filter

The proposed trickling filter model is a simplification of the model proposed by Nijhof (1995), it doesn't account for the growth of nitrifying bacteria and the plug flow dynamics in the trickling filter. It also assumes that the trickling filter is constantly filled with water, where actually only a fraction of the trickling filter is filled with water and most of it by air (Timmons and Ebeling, 2013). For a more precise model, all reactions taking place in the trickling filter need to be regarded, as well as the actual fluid dynamics.

Since the rate of nitrification depends on the TAN concentration. The performance of the trickling filter also is affected by the diurnal excretion variations. By modelling the trickling filter as five consecutive CSTRs the variations are buffered down. The use of a plug flow model with respect to the actual fluid dynamics would increase the model accuracy.

5.6. Settling Tank

The proposed settling tank model is strongly simplified, it neglects the retention time of the water and the settling time of sludge. Further it assumes no mixing, resuspension of settlements and immediate sludge removal. For futher improvement of the model all these factors need to be implemented. It was shown that the sludge removal efficiency depends on the particle size distribution. However no data on particle size distributions after drum filter backwashing was found. The estimated particle size distribution is based on few data and many assumptions (section 3.3.3).

The settling tank inflow is made up of the drum filter cake and backwash. The size of the cake varies with the concentration of TSS entering the drum filter. Diurnal excretion variations affect the settling tank by variations in the inflow. Shortly after feeding, when

the TSS concentration entering the drum filter peaks, also the inflow to the setlling tank peaks. The removal efficiency of the settling tank depends on the inflow, an increase in inflow results in a decrease of the removal efficiency. It is therefore the lowest shortly after feeding and increases afterwards.

5.7. General Conclusion

A model of the RAS loop of an aquaponic system was developed successfully. Model parameters were estimated based on literature findings. Due to the modularity of the model, it can easily be apllied to different system set ups. Special attention was given to the diurnal excretion dynamics of fish, it was shown that these variations affect the performance of each system module.

Particulate nutrient concentrations peak an hour after feeding, soluble nutrient concentrations around 2.5 hours later. A daily maximum is reached after the last feeding of the day. In decoupled aquaponic systems, where part of the recirculating flow is send to the hydroponic system, 3.5 hours after the last feeding of the day would be ideal time to send the water, for maximal soluble nutrient concentrations. In the present study however only the drum filter cake is send to the hydroponic system. Scarce knowledge about the composition of drum filter cakes is a bottleneck of the presented model.

The deterministic model was not able to accurately represent a comparable system. Implementing parameter uncertainties in the model is therefore recommended. Linear error propagation is not suitable. A Monte Carlo simulation with respect to parameter correlation is advised, to achieve general applicability of the model.

Bibliography

Allaman, I. B., R. V. R. Neto, R. T. F. de Freitas, T. A. Freato, A. de Assis Lago, A. C. Costa, and R. R. de Lima (2013). "Weight and morphometric growth of different strains of tilapia (Oreochromis sp)". In: *Revista Brasileira de Zootecnia* 42.5, pp. 305–311.

Aller Aqua (n.d.). *Tilapia - West Africa and Europe*. URL: `http://www.aller-aqua.com/species/warm-freshwater-species/tilapia-west-africa-europe`.

Amanico, A.L.L., J.H.V. Silva, J.B.K. Fernandes, N.K. Sakomoura, and G.R.B. Cruz (2014). "Use of mathematical models in the study of bodily growth in GIFT strain Nile tilapia". In: *Revista Ciência Agronômica* 45.2, pp. 257–266.

Bader, H. (1970). "The Hyperbolic Distribution of Particle Sizes". In: *Journal of Geophysical Research* 75.15, pp. 2822–2830.

Bergheim, A., S.J. Cripps, and H. Liltved (1998). "A system for the treatment of sludge from land-based fish-farms". In: *Aquatic Living Resources* 11.4, pp. 279–287.

Burton, D. and M. Burton (2017). *Essential fish biology : diversity, structure, and function*. Oxford: Oxford University Press, p. 417.

Chasiotis, H. (n.d.). *Nitrogen Excretion in Fish*. Lecture presentation. York University.

Chen, S., M.B. Timmons, D.J. Aneshansley, and Jr J.J. Bisogni (1993). "Suspended solids characteristics from recirculating aquacultural systems and design implications". In: *Aquaculture* 112, pp. 143–155.

DeLong, D.P., T.M. Losordo, and J.E. Rakocy (2009). "Tank Culture of Tilapia". In: 282.

Eding, E.H., A. Kamstra, J.A.J. Verreth, E.A. Huisman, and A. Klapwijk (2006). "Design and operation of nitrifying trickling filters in recirculating aquaculture: A review". In: *Aquacultural Engineering* (34), pp. 234–260.

FAO (2005). *Cultured Aquatic Species Information Programme. Oreochromis niloticus*. FAO Fisheries and Aquaculture Department. URL: `http://www.fao.org/fishery/cultured-species/Oreochromis_niloticus/en`.

— (2016). *The state of World Fisheries and Aquaculture 2016. Contributing to food security and nutrition for all*. Rome: Food and Agriculture Organization of the United Nations (FAO).

Fernandes, P.M., L.-F. Pedersen, and P.B. Pedersen (2014). "Daily micro particle distribution of an experimental recirculating aquaculture system — A case study". In: *Aquacultural Engineering* 60, pp. 28–34.

Goddek, S. (2017). "Opportunities and challenges of multi-loop aquaponic systems". PhD Thesis. Wageningen: Wageningen University.

Gómez-Pearanda, J. A. and L. C. Clavijo-Restrepo (2012). "Determination of the stomach emptying time of tilapia Oreochromis sp. using different weekly feeding frequencies and starvation". In: *Acta Agronómica* 61.3, pp. 219–223.

Grau, P., P. M. Sutton, S. Elmaleh, C. P. Grady, W. Gujer, M. Henze, and J. Koller (1983). "Recommended notation for use in the description of biological wastewater treatment processes". In: *Pure and Applied Chemistry* 55.6, pp. 1035–1040.

Gullian-Klanian, M. and C. Arámburu-Adame (2013). "Performance of Nile tilapia Oreochromis niloticus fingerlings in a hyper-intensive recirculating aquaculture system with low water exchange". In: *Latin American Journal of Aquatic Research* 41.1, pp. 150–162.

INAPRO (n.d.). *Project Overview*. URL: `http://www.inapro-project.eu/page/project-overview_p116/`.

Kamstra, A., J. W. van der Heul, and M. Nijhof (1998). "Performance and optimisation of trickling filters on eel farms". In: *Aquaculture Engineering* 17, pp. 175–192.

Karimanziraa, D., K.J. Keesman, W. Kloas, D. Baganz, and T. Rauschenbach (2016). "Dynamic modeling of the INAPRO aquaponic system". In: *Aquacultural Engineering* 75, pp. 29–45.

Kelly, L.A., A. Bergheim, and J. Stellwagen (1997). "Particle size distribution of wastes from freshwater fish farms". In: *Aquaculture International* 5, pp. 65–67.

Kloas, W. et al. (2015). "A new concept for aquaponic systems to improve sustainability, increase productivity, and reduce environmental impacts". In: *Aquaculture Environment Interactions* 7.2, pp. 179–192.

Kunkel, R., S. Hannappel, H. J. Voigt, and F. Wendland (2002). *Die natürliche Grundwasser beschaffenheit ausgewählter hydrostratigrafischer Einheiten in Deutschland*. German. Forschungszentrum Jülich GmbH, Programmgruppe Systemforschung und Technologische Entwicklung.

Lewis, W.M., J.H. Yopp, H.L. Schramm, and A.M. Brandenburg (1978). "Use of Hydroponics to Maintain Quality of Recirculated Water in a Fish Culture System". In: *Transactions of the American Fisheries Society* 107.1, pp. 92–99.

Losordo, T.M., A.O. Hobbs, and D.P. DeLong (2000). "The design and operational characteristics of the CP&L:EPRI fish barn: a demonstration of recirculating aquaculture technology". In: *Aquacultural Engineering* 22, pp. 3–16.

Love, D.C., J.P. Fry, E.S. Li X. Hill, L. Genello, K. Semmens, and R.E. Thompson (2015). "Commercial aquaponics production and profitability: Findings from an international survey". In: *Aquaculture* 435, pp. 67–74.

Monsees, H., W. Kloas, and S. Wuertz (2017). "Decoupled systems on trial: Eliminating bottlenecks to improve aquaponic processes". In: *Plos One* 12.9.

Neto, R.M. and A. Ostrensky (2015). "Nutrient load estimation in the waste of Nile tilapia Oreochromis niloticus (L.) reared in cages in tropical climate conditions". In: *Aquaculture Research* 46, pp. 1309–1322.

Nijhof, M. (1995). "Bacterial stratification and hydraulic loading effects in a plug-flow model for nitrifying trickling filters applied in recirculating fish culture systems". In: *Aquaculture* 134, pp. 49–64.

Obirikorang, K.A., S. Amisah, S. C. Fialor, and P.V. Skov (2015). "Digestibility and postprandial ammonia excretion in Nile tilapia (Oreochromis niloticus) fed diets containing different oilseed by-products". In: *Aquaculture International* 23, pp. 1249–1260.

Obirikorang, K.A., S. Amisah, and P.V. Skov (2017). "Effect of some common West African farm-made feeds on the oxygen consumption and ammonia excretion rates of Nile

tilapia, Oreochromis niloticus". In: *Marine and freshwater behaviour and physiology* 50.3, pp. 219–232.

Patterson, R.N. and K.C. Watts (2003). "Micro-particles in recirculating aquaculture systems: microscopic examination of particles". In: *Aquacultural Engineering* 28, pp. 115–130.

Patterson, R.N., K.C. Watts, and T.A. Gill (2003). "Micro-particles in recirculating aquaculture systems: determination of particle density by density gradient centrifugation". In: *Aquacultural Engineering* 27, pp. 105–115.

Patterson, R.N., K.C. Watts, and M.B. Timmons (1999). "The power law in particle size analysis for aquacultural facilities". In: *Aquacultural Engineering* 19, pp. 259–273.

Rakocy, J. E. (2012). "Aquaponics — Integrating Fish and Plant Culture". In: *Aquaculture Production Systems*. Ed. by J. Tidwell. 1st ed. John Wiley & Sons, Inc.

Rakocy, J.E. (1989). "Tank Culture of Tilapia". In: 282.

Reyes Lastiri, D., C. Geelen, H. J. Cappon, H. Rijnaarts, D. Baganz, W. Kloas, D. Karimanzira, and K. J. Keesman (2018). "Model of water and nutrient cycles in an aquaponic system for resource efficient design and operation". In: *Aquacultural Engineering* 83, pp. 27–39.

Reyes Lastiri, D., T. Slinkert, H.J. Cappon, D. Baganz, G. Staaks, and K.J. Keesman (2016). "Model of an aquaponic system for minimised water, energy and nitrogen requirements". In: *Water Science & Technology* 74.1, pp. 30–37.

Riche, M., D.I. Haley, M. Oetker, S. Garbrecht, and D.L. Garling (2004). "Effect of feeding frequency on gastric evacuation and the return of appetite in tilapia Oreochromis niloticus (L.)" In: *Aquaculture* 234, pp. 657–673.

Richter, H., C. Lückstädt, U. Focken, and K. Becker (2003). "Evacuation of pelleted feed and the suitability of titanium(IV) oxide as a feed marker for gut kinetics in Nile tilapia". In: *Journal of Fish Biology* 63, pp. 1080–1099.

Ross, J. (1998). *Hydroponic tomato production : a practical guide to growing tomatoes in containers*. Casper Publications.

Santos, V.B. dos, E. Yoshihara, R.T.F. Freitas, and R.V.R Neto (2008). "Exponential growth model of Nile tilapia (Oreochromis niloticus) strains considering heteroscedastic variance". In: *Aquaculture* 274, pp. 96–100.

Schneider, O., A.K. Amirkolaie, J. Vera-Cartas, E.H. Eding, J.W. Schrama, and J.A.J. Verreth (2004). "Digestibility, faeces recovery, and related carbon, nitrogen and phosphorus balances of five feed ingredients evaluated as fishmeal alternatives in Nile tilapia, Oreochromis niloticus L." In: *Aquaculture Research* 35, pp. 1370–1379.

Seawright, D.E., R.R. Stickney, and R.B. Walker (1998). "Nutrient dynamics in integrated aquaculture–hydroponics systems". In: *Aquaculture* 160, pp. 215–237.

Stokic, J. (2012). "Particle size distribution in the Tilapia Recirculating Aquaculture System". MSc Thesis. Department of Mathematical Sciences and Technology, University of Life science in Ås, Norway.

Timmons, M.B. and J.M. Ebeling, eds. (2013). *Recirculating aquaculture*. 3rd ed. Ithaca, NY: Ithaca Publishing Company.

Tucker, C.S. and J.A. Hargreaves, eds. (2008). *Environmental Best Management Practices for Aquaculture*. 1st ed. 2121 State Avenue, Ames, Iowa 50014, USA: Blackwell Publishing Professional.

Wik, T.E.I., B.T. Lindén, and P.I. Wramner (2009). "Integrated dynamic aquaculture and wastewater treatment modelling for recirculating aquaculture systems". In: *Aquaculture* 287, pp. 361–370.

Wing-Keong, N. and N. Romano (2013). "A review of the nutrition and feeding management of farmed tilapia throughout the culture cycle". In: *Reviews in Aquaculture* 5, pp. 220–254.

A. Appendix 1 - Data

A.1. Feed Composition Data

Table A.1.: References and datasets used for feed composition parameters (section 2.1); Feed components given in g/kg wet feed.

Feed component	Schneider et al. (2004)						Neto and Ostrensky (2015)				Seawright et al. (1998)	Mean	SE of means
	WGD	SBE	SBM	DWD	SCP	FMD	Fry	Juv	Gro	Ter			
Dry matter	870.20	872.20	868.20	863.90	866.50	868.30	906.04	904.72	902.26	902.18	917.00	885.59	19.48
Protein	347.10	357.10	304.70	274.60	291.10	325.20	399.6	352.28	276.68	240.78	416.00	325.92	51.90
C	410.50	409.70	400.60	390.40	394.20	400.40						400.97	7.36
N	55.50	57.10	48.80	43.90	46.60	52.00	61.48	54.20	42.57	37.04	64.00	51.20	7.91
P	9.70	10.20	10.20	12.10	11.70	13.00	15.59	15.03	11.74	11.48	16.14	12.44	2.14
K											13.96	13.96	0.00
Ca							27.39	24.53	28.49	19.61	17.56	23.52	4.28
Mg											3.27	3.27	0.00
Na											5.13	5.13	0.00

Schneider et al. (2004), feed compositions for four different diets: WGD, wheat gluten diet; SBE, soybean extract diet; SBM, soybean meal diet; DWD, duckweed diet; SCP, single-cell protein diet; FMD, fishmeal diet;
Neto and Ostrensky (2015), feed compositions for four different growth stages: Fry: fry; Juv: juvenile; Gro: growth; Ter: termination.

A.2. Daily Feeding Ratio Calibration Data

Table A.2.: References and datasets used for daily feeding ratio calibration (section 3.1); Daily feeding ratio (DFR) given as fraction of fish weight per day (wet weight), depending on fish weight (m_{fish} in g).

DeLong et al. (2009)		J. Rakocy (1989)		Wing-Keong and Romano (2013)		Aller Aqua (n.d.) Aller Sana		Aller Orea		Aller Futura		Aller Pravo	
m_{fish}	DFR	m_{fish}	DFR	m_{fish}	DFR	m_{fish}	DFR	m_{fish}	DFR	m_{fish}	DFR	m_{fish}	DFR
0.02	0.2	0.02	0.2	0.5	0.2	30	0.0327	60	0.0324	0.5	0.0828	0.3	0.1334
0.5	0.15	0.075	0.15	1	0.15	60	0.0327	100	0.0324	1	0.0828	0.5	0.1334
5	0.1	5	0.1	1	0.11	60	0.0272	100	0.0259	1	0.0679	0.5	0.1094
18	0.05	20	0.07	2	0.065	100	0.0272	200	0.0259	3	0.0679	1	0.1094
75	0.03	50	0.04	10	0.065	100	0.0218	200	0.0208	3	0.0556	1	0.0896
150	0.03	100	0.035	15	0.046	200	0.0218	400	0.0208	6	0.0556	3	0.0896
150	0.015	250	0.015	30	0.035	200	0.0174	400	0.0166	6	0.0456	3	0.0735
450	0.015	450	0.01	60	0.03	400	0.0174	800	0.0166	10	0.0456	6	0.0735
				100	0.025	400	0.0139	800	0.0133	10	0.0374	6	0.0602
				175	0.021	800	0.0139			30	0.0374	10	0.0602
				300	0.018	800	0.0112			30	0.0306		
				400	0.015					60	0.0306		

Allaman et al. (2013), growth data of four different tilapia strains cultured in raceways: Red strain; UFLA, tilapia cultured at fish growth station of Universidade Federal de Lavras (UFLA); Thai strain; Commerial, genetically improved strain (GIFT);
Amanico et al. (2014), growth data of tilapia (GIFT) cultured in brick tanks;
Santos et al. (2008), growth data of two diggerent tilapia strains cultured in cages: Thai starain; Commercial, GIFT;
Gullian-Klanian and Arámburu-Adame (2013), growth data from tilapia cultured at three different densities in RAS (same time line applies for all measurements): D400, 400 fish per m^3; D500, 500 fish per m^3; D600, 600 fish per m^3.

A.3. Growth Calibration Data

Table A.3.: References and datasets used for ideal growth calibration of feeder module (section 3.1), and uptake calibration of fish module (section 3.2); Time given as days after stocking; Fish weight (m_{fish}) given in g.

Allaman et al. (2013)								Amanico et al. (2014)		Santos et al. (2008)				Gullian-Klanian and Arámburu-Adame (2013)			
Red		UFLA		Thai		Commercial				Thai		Commercial		D400		D500	D600
Time	m_{fish}	Time	m_{fish}	Time	m_{fish}	Time	m_{fish}	Time	m_{fish}	Time	m_{fish}	Time	m_{fish}	Time	m_{fish}	m_{fish}	m_{fish}
0	35.03	0	24.14	0	27.13	0	34.78	0	7.42	1	9.86	1	9.33	0	1.60	1.63	1.31
27	41.40	27	31.03	28	46.51	29	60.87	15	8.93	25	24.64	34	25.25	7	4.90	4.50	4.86
54	63.69	53	51.72	56	58.14	57	104.35	30	12.72	74	83.75	75	90.93	14	6.89	7.20	7.83
81	95.54	81	103.45	83	58.14	84	95.65	45	16.50	116	157.59	115	162.73	21	1.63	1.65	1.31
108	76.43	108	93.10	111	62.02	112	121.74	60	27.10	158	237.85	136	213.01	28	17.93	17.85	16.65
135	121.02	135	103.45	140	158.91	140	230.43	75	37.69					35	24.31	22.55	24.57
162	117.83	162	155.17	166	178.29	167	330.43	90	52.83					42	34.12	31.66	35.55
189	238.85	189	224.14	195	306.20	195	365.22	105	101.27					49	46.60	41.83	45.06
216	267.52	216	386.21	222	337.21	223	543.48	120	184.53					56	54.99	52.51	58.08
244	493.63	243	503.45	250	418.60	251	617.39	135	229.94					63	62.26	60.57	57.25
								150	296.55					70	71.93	57.79	69.54
								165	367.70								
								180	425.98								

Aller Aqua (n.d.), feeding recommondations of a commercial feed supplier for four different feed types: Aller Sans, Aller Orea, Aller Futra and Aller Pravo.

A.4. Balance between Uptake, Faeces and Urine Data

Table A.4.: References and datasets used for uptake ratios given as percentage of consumed feed component (see table 2.3).

Feed component	Schneider et al. (2004)						Neto and Ostrensky (2015)				Seawright et al. (1998)				Mean	SE of means
	WGD	SBE	SBM	DWD	SCP	FMD	Fry	Juv	Gro	Ter	BM151	BM377	BM902	BM1804		
C	34.60	34.20	32.40	32.50	30.20	35.80									32.28	1.82
N	43.10	44.20	45.10	48.00	44.20	48.00	43.25	43.25	43.25	43.25	42.00	43.00	47.00	44.00	44.40	1.85
P	68.50	70.40	64.00	62.50	60.60	63.30	34.07	34.07	34.07	34.07	51.00	54.00	59.00	55.00	53.18	13.08
K											23.00	24.00	26.00	24.00	24.25	1.09
Ca							36.96	36.96	36.96	36.96					36.96	0.00
Mg											19.00	20.00	22.00	21.00	20.50	1.12
Na											57.00	48.00	52.00	43.00	50.00	5.15

Schneider et al. (2004), uptake ratios for four different diets: WGD, wheat gluten diet; SBE, soybean extract diet; SBM, soybean meal diet; DWD, duckweed diet; SCP, single-cell protein diet; FMD, fishmeal diet;
Neto and Ostrensky (2015), uptake ratios for four different growth stages: Fry: fry; Juv: juvenile; Gro: growth; Ter: termination
Seawright et al. (1998), uptake ratios for four different fish densities: BM151: 151 g of fish per system; BM377: 377 g of fish per system; BM902: 902 g of fish per system; BM1804: 1804 g of fish per system.

Table A.5.: References and datasets used for faeces ratios given as percentage of consumed feed component (see table 2.3).

Feed component	Schneider et al. (2004)						Neto and Ostrensky (2015)				Seawright et al. (1998)				Mean	SE of means
	WGD	SBE	SBM	DWD	SCP	FMD	Fry	Juv	Gro	Ter	BM151	BM377	BM902	BM1804		
Dry matter	19.2	29.8	20.8	22.4	22.5	20.9	27.74	27.56	29.38	29.1					24.94	3.93
C	14.20	14.40	15.80	15.30	17.60	15.30									15.43	1.11
N	7.40	8.60	9.50	11.10	10.90	10.40	13.70	12.42	13.88	18.33	15.00	10.00	7.00	8.00	11.16	3.10
P	35.00	35.50	35.50	32.90	38.10	40.10	37.84	40.59	45.06	46.95	51.00	54.00	59.00	55.00	43.32	8.22
K											6.00	5.00	3.00	3.00	4.25	1.30
Ca							28.55	31.55	18.39	25.91					26.10	4.88
Mg											24.00	19.00	17.00	14.00	18.50	3.64
Na											19.00	12.00	11.00	10.00	13.00	3.54

See subcaption table A.4.

Table A.6.: References and datasets used for urine ratios given as percentage of consumed feed component (see table 2.3).

Feed component	Schneider et al. (2004)						Neto and Ostrensky (2015)				Seawright et al. (1998)				Mean	SE of means
	WGD	SBE	SBM	DWD	SCP	FMD	Fry	Juv	Gro	Ter	BM151	BM377	BM902	BM1804		
C	51.20	51.40	51.80	52.20	52.20	48.90									51.28	1.13
N	49.50	47.20	45.40	40.90	44.90	41.60	43.05	44.33	42.87	38.42	43.00	47.00	46.00	48.00	44.44	2.92
P	-3.50	-5.90	0.50	4.60	1.30	-3.40	28.09	25.34	20.87	18.98	-2.00	-8.00	-18.00	-10.00	3.49	13.71
K											71.00	71.00	71.00	73.00	71.50	0.87
Ca							34.49	31.49	44.65	37.13					36.94	4.88
Mg											57.00	61.00	61.00	65.00	61.00	2.83
Na											24.00	40.00	37.00	47.00	37.00	8.34

See subcaption table A.4.

A.5. Digestive Tract Evacuation Calibration Data

Table A.7.: References and datasets used for digestive tract evacuation calibration (section 3.2.1); Time given as hours after feeding; Relative digestive tract content ($\frac{m_{digestive}}{m_{feed}}$) given in g/g.

Richter et al. (2003)					Riche et al. (2004)			Gómez-Pearanda and Clavijo-Restrepo (2012)							
Set 1		Set 2		Set 3	Set 1		Set 2	Set 1		Set 2	Set 3	Set 4		Set 5	Set 6
Time	$\frac{m_{digestive}}{m_{feed}}$	Time	$\frac{m_{digestive}}{m_{feed}}$	$\frac{m_{digestive}}{m_{feed}}$	Time	$\frac{m_{digestive}}{m_{feed}}$	$\frac{m_{digestive}}{m_{feed}}$	Time	$\frac{m_{digestive}}{m_{feed}}$	$\frac{m_{digestive}}{m_{feed}}$	$\frac{m_{digestive}}{m_{feed}}$	Time	$\frac{m_{digestive}}{m_{feed}}$	$\frac{m_{digestive}}{m_{feed}}$	$\frac{m_{digestive}}{m_{feed}}$
0.25	0.7360	0.25	0.8125	0.9155	0	0.9968	0.9992	0	1.0000	1.0000	1.0000	0	1.0000	1.0000	1.0000
0.7	0.6193	1.25	0.8010	0.8556	0.5	0.8758	0.8323	2	0.4422	0.7590	0.4423	2	0.7729	0.6454	0.7436
1.15	0.5647	2.25	0.7157	0.8021	1	0.6823	0.6605	4	0.2590	0.5199	0.2782	4	0.2032	0.2948	0.3256
1.6	0.5395	3.25	0.5040	0.5438	2	0.5492	0.4065	6	0.0299	0.0478	0.0718	6	0.1633	0.1932	0.1308
2.05	0.5818	4.25	0.6351	0.7055	4	0.4016	0.2855					8	0.1594	0.1614	0.1102
2.5	0.5920	5.25	0.5524	0.5732	6	0.3194	0.1718								
2.95	0.4295	7.25	0.4078	0.4378	8	0.2516	0.1500								
3.4	0.4959	9.25	0.3808	0.4619	12	0.1960	0.1113								
3.85	0.4500				18	0.0508	0.0605								
4.75	0.4661														
5.7	0.4486														
6.6	0.2903														
7.5	0.2745														
8.4	0.1991														
9.3	0.1254														

Richter et al. (2003), tilapia body weight = 200-300 g (same time line for set 2 and 3): Set 1, control measurent, DFR=0.5%, stomach content weight after disection; Set 2, DFR=0.5%, stomach content weight after disection; Set 3, DFR=0.5%, marker in stomach weight after disection;
Riche et al. (2004), tilapia body weight = 183 g (same time line for set 1 and 2): Set 1, DFR=2.1%, feeding frequencie = 5 times per day; Set 2, DFR=2.1%, feeding frequencie = 3 times per day;
Gómez-Pearanda and Clavijo-Restrepo (2012), tilapia body weight = 150 g (same time line for set 1, 2, and 3, and set 4, 5, and 6): Set 1, fed according to feed supplier recommondations, first feeding of the day; Set 2, fed according to satuation, first feeding of the day; Set 3, fed to satuation six days per week, first feeding of the day; Set 4, same as Set 1, seccond feeding of the day; Set 5, same as Set 2, seccond feeding of the day; Set 6, same as Set 3, seccond feeding of the day.

A.6. Urinal Tract Evacuation Calibration Data

Table A.8.: Reference and datasets used for urinal tract evacuation calibration (section 3.2.1); Time given as hours after feeding; Soluble N excretion given as percentage of cumulative soluble N excretion relative to N intake via feed.

	Obirikorang et al. (2015)				Adapted			
	CTRL	CM	PKM	SBM	CTRL	CM	PKM	SBM
Time	Soluble N excretion	Soluble N excretion	Soluble N excretion	Soluble N excretion	Soluble N excretion	Soluble N excretion	Soluble N excretion	Soluble N excretion
0	2.31	2.51	2.89	2.13	-0.49	0.03	1.01	-0.96
1	2.98	2.98	3.57	2.78	1.25	1.25	2.78	0.73
2	4.15	4.47	4.62	3.71	4.29	5.12	5.51	3.15
4	6.78	7.05	6.81	5.99	11.13	11.83	11.21	9.07
6	10.79	10.82	10.06	9.06	21.55	21.63	19.66	17.06
9	14.44	13.95	12.40	11.29	31.04	29.77	25.74	22.85
12	16.28	15.44	13.39	13.36	35.83	33.64	28.31	28.24
16	17.60	16.43	14.06	14.82	39.26	36.22	30.06	32.03
24	20.79	17.25	14.38	15.55	47.55	38.35	30.89	33.93

Obirikorang et al. (2015), soluble N excretion of tilapia (body weight = 50 g) fed with four different diets: CTRL, control diet; CM, copra meal diet; PKM, palm kernel meal diet; SBM, soybean meal diet;
Data used for urinal tract evacuation calibration was adapted from Obirikorang et al. (2015), as explained in section 3.2.1.

B. Appendix 2 - Model Parameter List

Appendix B holds a list of model parameters used in full system simulation (section 4.2), including values, units, descriptions, and references.

Water				
ρ_{water}	1.00	g/mL	Density of water	-
$S_{C,fresh}$	0.00	g/ml	Soluble C in fresh water	-
$S_{TAN,fresh}$	0.15	g/ml	Soluble ammonia in fresh water	Kunkel et al. (2002)
$S_{NO3,fresh}$	0.10	g/ml	Soluble nitrate in fresh water	Kunkel et al. (2002)
$S_{P,fresh}$	0.00	g/ml	Soluble P in fresh water	-
$S_{K,fresh}$	2.30	g/ml	Soluble K in fresh water	Kunkel et al. (2002)
$S_{Ca,fresh}$	69.00	g/ml	Soluble Ca in fresh water	Kunkel et al. (2002)
$S_{Mg,fresh}$	10.00	g/ml	Soluble Mg in fresh water	Kunkel et al. (2002)
$S_{Na,fresh}$	0.00	g/ml	Soluble Na in fresh water	-
TSS_{fresh}	0.00	g/ml	Total solids concentration in fresh water	-
$X_{C,fresh}$	0.00	g/ml	Particulate C in fresh water	-
$X_{C,fresh}$	0.00	g/ml	Particulate N in fresh water	-
$X_{C,fresh}$	0.00	g/ml	Particulate P in fresh water	-
$X_{C,fresh}$	0.00	g/ml	Particulate K in fresh water	-
$X_{C,fresh}$	0.00	g/ml	Particulate Ca in fresh water	-
$X_{C,fresh}$	0.00	g/ml	Particulate Mg in fresh water	-
$X_{C,fresh}$	0.00	g/ml	Particulate Na in fresh water	-
Feeder module				
$\mathrm{d}t_{feeder}$	15	min	Feeder simulation time step	User set
n_{fish}	1000	$-$	Total number of fish	Monsees et al. (2017)
$m_{0,fish}$	$1000 * 66.9$	g	Initial mass of all fish	Monsees et al. (2017)
$daily\_feed\_schedule$	7, 12, 17	hr	Times at which feed is distributed daily	User set
DM_{feed}	0.8859	g/g	Dry matter fraction of feed	See table A.1
C_{feed}	0.4010	g/g	C fraction of feed	See table A.1
N_{feed}	0.0512	g/g	N fraction of feed	See table A.1
P_{feed}	0.0124	g/g	P fraction of feed	See table A.1
K_{feed}	0.0140	g/g	K fraction of feed	See table A.1

Ca_{feed}	0.0235	g/g	Ca fraction of feed	See table A.1
Mg_{feed}	0.0033	g/g	Mg fraction of feed	See table A.1
Na_{feed}	0.0051	g/g	Na matter fraction of feed	See table A.1
a_{DFR}	0.093	$1/g/day$	Daily feeding ratio constant	Calibrated in section 3.1
b_{DFR}	-0.28	$-$	Daily feeding ratio constant	Calibrated in section 3.1
a_{growth}	0.24	g/day	Ideal growth model constant	Calibrated in section 3.1
b_{growth}	0.0075	g/day^2	Ideal growth model constant	Calibrated in section 3.1
Fish module				
$\mathrm{d}t_{fish}$	15	min	Fish simulation time step	User set
n_{fish}	1000	$-$	Total number of fish	Monsees et al. (2017)
$m_{0,fish}$	$1000 * 66.9$	g	Initial mass of all fish	Monsees et al. (2017)
$\tau_{digestive}$	4.5465	hr	Digestive tract evacuation time constant	Calibrated in section 3.2
τ_{urinal}	4.5091	hr	Urinal tract evacuation time constant	Calibrated in section 3.2
DM_{fish}	0.3058	g/g	Dry matter fraction fish	Schneider et al. (2004) and Neto and Ostrensky (2015)
ρ_{faeces}	1.05	g/ml	Density of tilapia faeces	Timmons and Ebeling (2013)
k_{uptake}	0.2036	g/g	Fraction of feed (dry weight) taken up	Calibrated in section 3.2
k_{faeces}	0.2494	g/g	Fraction of feed (dry weight) excreted as faeces	See table A.5
k_{urine}	$1 - k_{uptake} - k_{faeces}$	g/g	Fraction of feed (dry weight) excreted as urine	-
kC_{uptake}	0.3328	g/g	C fraction (dry weight) taken up	See table A.4
kC_{faeces}	0.1543	g/g	C fraction (dry weight) excreted as faeces	See table A.5
kC_{urine}	$1 - C_{uptake} - C_{faeces}$	g/g	C fraction (dry weight) excreted as urine	-
kN_{uptake}	0.4440	g/g	N fraction (dry weight) taken up	Calibrated in section 3.2
kN_{faeces}	0.1116	g/g	N fraction (dry weight) excreted as faeces	See table A.5
kN_{urine}	$1 - kN_{uptake} - kN_{faeces}$	g/g	N faction (dry weight) excreted as urine	See table A.6
k_{TAN}	0.9	g/g	Ammonia fraction of urine N	Timmons and Ebeling (2013)
kP_{uptake}	0.5318	g/g	P fraction (dry weight) taken up	See table A.4
kP_{faeces}	0.4332	g/g	P fraction (dry weight) excreted as faeces	See table A.5
kP_{urine}	$1 - kP_{uptake} - kP_{faeces}$	g/g	P fraction (dry weight) excreted as urine	See table A.6
kK_{uptake}	0.2425	g/g	K fraction (dry weight) taken up	See table A.4
kK_{faeces}	0.0425	g/g	K fraction (dry weight) excreted as faeces	See table A.5
kK_{urine}	$1 - kK_{uptake} - kK_{faeces}$	g/g	K fraction (dry weight) excreted as urine	See table A.6
kCa_{uptake}	0.3696	g/g	Ca fraction (dry weight) taken up	See table A.4
kCa_{faeces}	0.2610	g/g	Ca fraction (dry weight) excreted as faeces	See table A.5
kCa_{urine}	$1 - kCa_{uptake} - kCa_{faeces}$	g/g	Ca fraction (dry weight) excreted as urine	See table A.6
kMg_{uptake}	0.2050	g/g	Mg fraction (dry weight) taken up	See table A.4
kMg_{faeces}	0.1850	g/g	Mg fraction (dry weight) excreted as faeces	See table A.5
kMg_{urine}	$1 - kMg_{uptake} - kMg_{faeces}$	g/g	Mg fraction (dry weight) excreted as urine	See table A.6

kNa_{uptake}	0.5000	g/g	Na fraction (dry weight) taken up	See table A.4
kNa_{faeces}	0.1300	g/g	Na fraction (dry weight) excreted as faeces	See table A.5
kNa_{urine}	$1 - kNa_{uptake} - kNa_{faeces}$	g/g	Na fraction (dry weight) excreted as urine	See table A.6
Fish tank module				
$\mathrm{d}t_{FT}$	15	min	Fish tank simulation time step	User set
V_{FT}	6.8	m^3	Total fish tank volume	Monsees et al. (2017)
$f_{V,FT,out}$	6.8	m^3/hr	Volumetric flow out of fish tank	Losordo et al. (2000)
Drum filter module				
$\mathrm{d}t_{DF}$	15	min	Drum filter simulation time step	User set
a_{DF}	0.8300	$\%$	Drum filter efficiency constant	Calibrated in section 3.3
b_{DF}	0.3020	L/mg	Drum filter efficiency constant	Calibrated in section 3.3
c_{DF}	-2.2867	mg/L	Drum filter efficiency constant	Calibrated in section 3.3
$backwash\_ratio$	0.001	$\frac{m^3/hr}{m^3/hr}$	Backwash flow relative to drum filter inflow	Tucker and Hargreaves (2008)
TSS_{cake}	3.26	g/L	Solids concentration in cake	See section 3.3.2
Trickling filter module				
$\mathrm{d}t_{DF}$	15	min	Trickling filter simulation time step	User set
$n_{TF,CSTR}$	5	$-$	Number of CSTRs	User set
$V_{TF,CSTR}$	2	m^3	Volume of one CSTR	Kamstra et al. (1998)
$A_{TF,CS}$	5	m^2	Cross sectional area of trickling filter	Kamstra et al. (1998)
SSA_{TF}	5	m^2/m^3	Specific surface area of trickling filter medium	Kamstra et al. (1998)
ε_{TF}	0.9	m^3/m^3	Void fraction of trickling filter medium	Kamstra et al. (1998)
a_{rTAN}	$7.81 * 10^{-4} * \frac{f_{V,TF,in}}{A_{TF,CS}}$	$g/m^2/day$	Ammonia reaction rate constant	Nijhof (1995)
b_{rTAN}	0.2	$g/m^2/day$	Ammonia reaction rate constant	Nijhof (1995)
c_{rTAN}	0.7	$g/m^2/day$	Ammonia reaction rate constant	Nijhof (1995)
Settling tank module				
$\mathrm{d}t_{ST}$	15	min	Settling tank simulation time step	User set
β_{ST}	3.35	$-$	β-value of particle size distribution in ST inflow	See section 3.4
A_{ST}	5	m^2	Settling zone area of settling tank	Bergheim et al. (1998)
TSS_{sludge}	75	mg/L	Solids concentration in sludge	(Tucker and Hargreaves, 2008)